

# Recent Results from the Graal Beam

Carlo Schaerf

Dipartimento di Fisica

Università degli Studi di Roma "Tor Vergata"

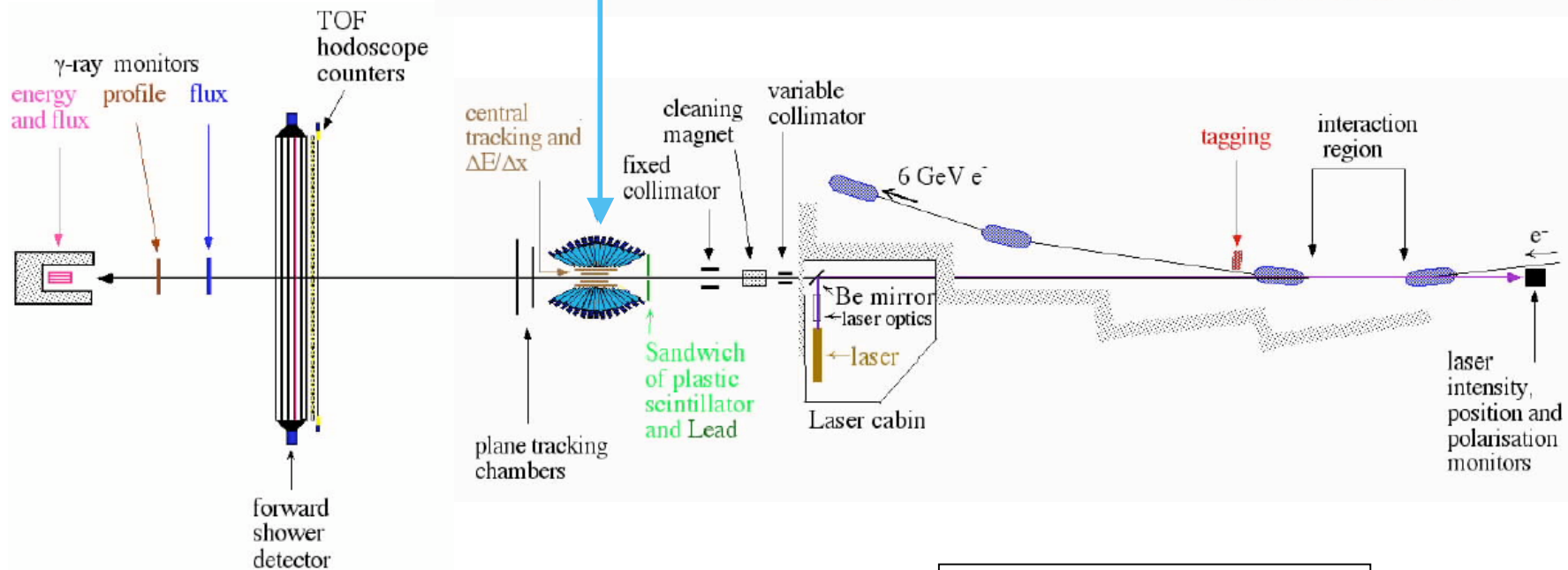
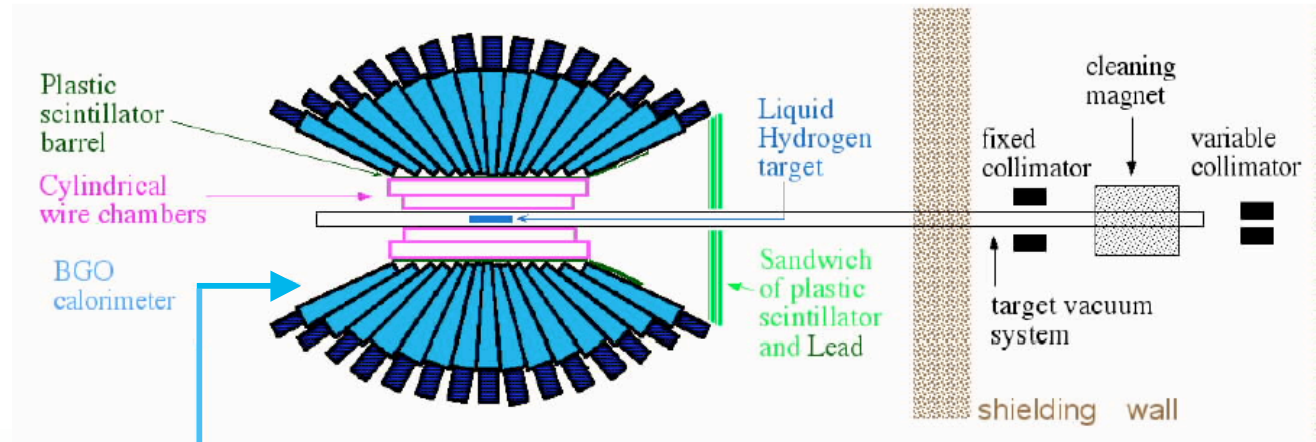
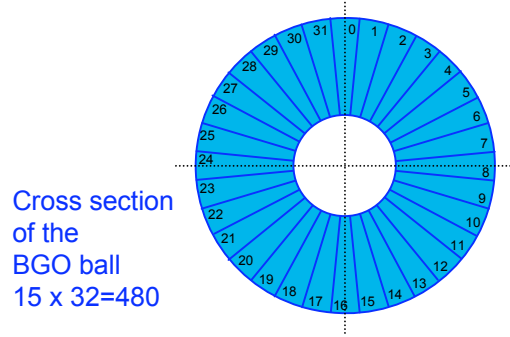
INFN - Sezione di Roma "Tor Vergata"

for the Graal collaboration

Sixth International Conference  
on  
Perspectives in Hadronic Physics

ICTP - Trieste, May 12-16, 2008

# Graal Apparatus

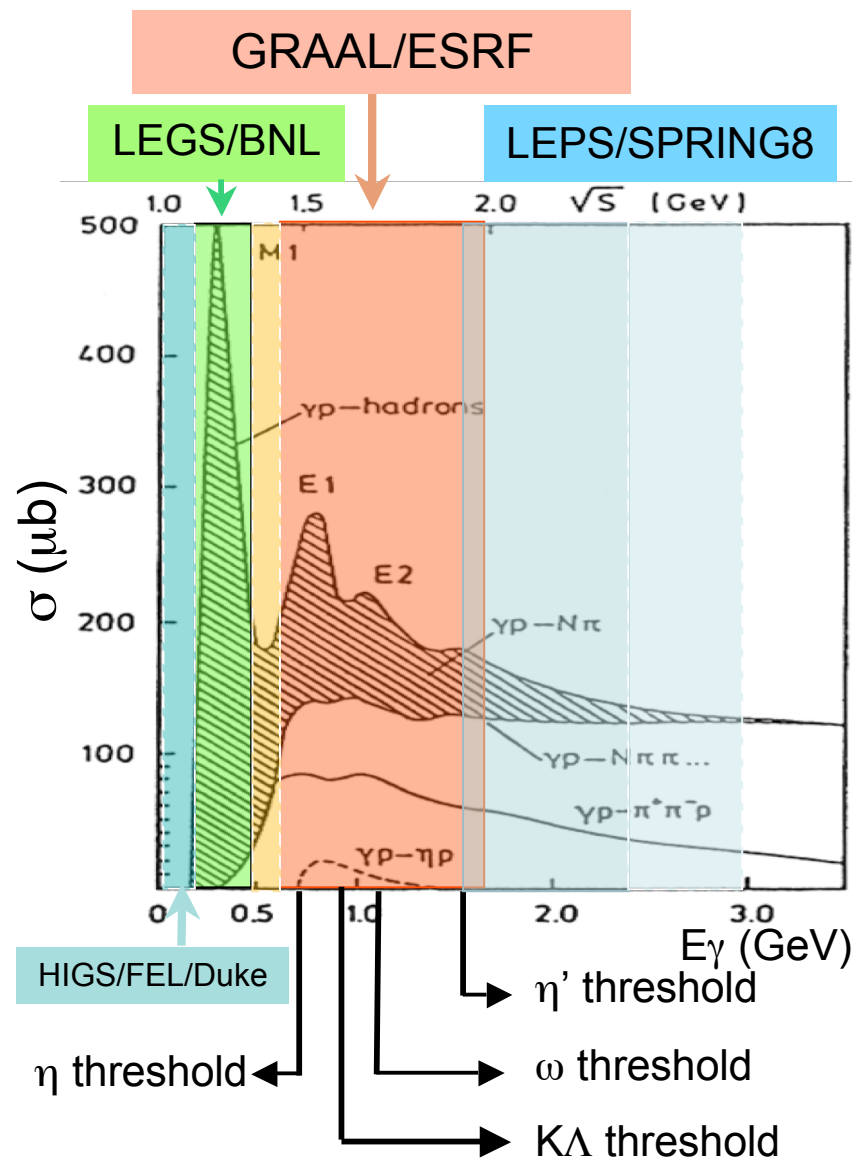


NOT IN SCALE

**Table. Ladon beams worldwide**

Project name	Ladon	Taladon	ROKK-1M	LEGS	LEGS-2	Graal	LEPS	HIGS
Location	Frascati, Italy		Novosibirsk, Russia	Brookhaven, US		Grenoble, France	Harima, Japan	Durham, UK
Storage ring	Adone	Adone	VEPP-4M	NSLS	NSLS	ESRF	SPring-8	TUNL-FEL
Energy defining method	Collimation	Internal tagging	Tagging	External tagging	External tagging	Internal tagging	Internal tagging	Collimation
Electron energy (GeV)	1.5	1.5	1.4–5.3	2.5	2.8	6.04	8	1.0
Laser photon energy (eV)	2.45	2.45	1.17–3.51	3.53	4.71	3.53	3.53	8.2
Gamma-ray energy (MeV)	5–80	35–80	100–1200	180–320	285–470	550–1470	1500–2400	5–225
Energy resolution (%)	1.4–10	5	—	1.6	1.1	1.1	1.25	1
Energy spread (FWHM, MeV)	0.07–8	4–2	—	5	5	16	30	—
Electron current	0.1	0.1	0.1	0.2	0.2	0.2	0.1	100
Gamma intensity $s^{-1}$	$10^5$	$5 \times 10^5$	$2 \times 10^6$	$4 \times 10^6$	$2 \times 10^6$	$2 \times 10^6$	$2 \times 10^6$	$10^6$ – $10^8$
First year of operation	1978	1989	1993	1987	1999	1996	1999	1996

# Ladon Beams in the World



• Graal:

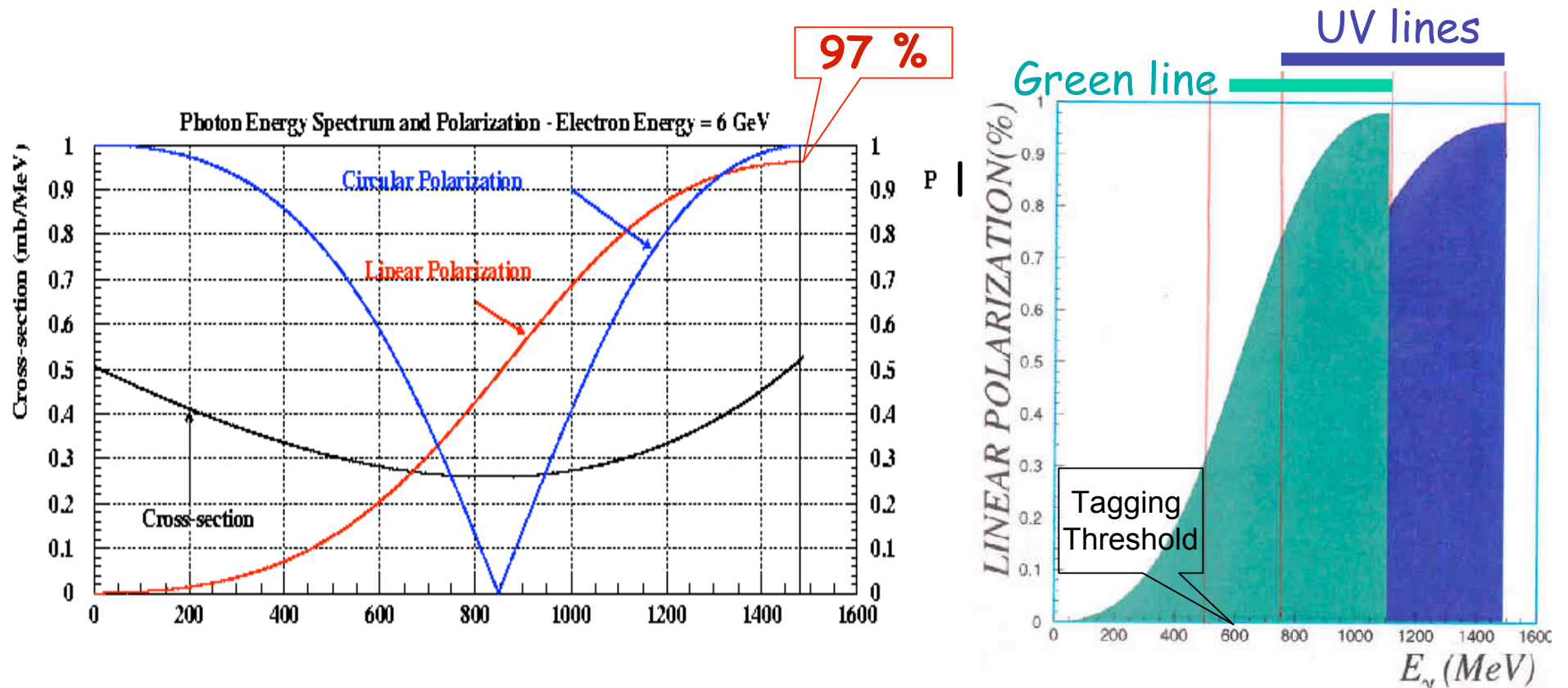
•  $E_\gamma = .6-1.5$  GeV /  $W=1.4-1.9$  GeV

• Region of the second and third baryon resonances

•  $\eta$ ,  $K$ ,  $\omega$ ,  $\eta'$  thresholds

• Complementary of HIGS, LEGS, Graal and LEPS

# Polarization of the Graal beam



At maximum gamma-ray energy the polarization is very close to that of the laser. Changing the laser line changes the polarization of the gamma-ray beam at a given energy.

# Graal Experimental Program

Finished

$$\vec{\gamma} + p \rightarrow \pi^0 + p$$

$$\vec{\gamma} + p \rightarrow \eta + p$$

$$\vec{\gamma} + p \rightarrow \pi^+ + n$$

$$\vec{\gamma} + p \rightarrow \pi^0 + \pi^0 + p$$

$$\vec{\gamma} + p \rightarrow \pi^0 + \eta + p$$

$$\vec{\gamma} + p \rightarrow k^+ + \Lambda$$

$$\vec{\gamma} + p \rightarrow k^+ + \Sigma^0$$

$$\vec{\gamma} + n \rightarrow \eta + n$$

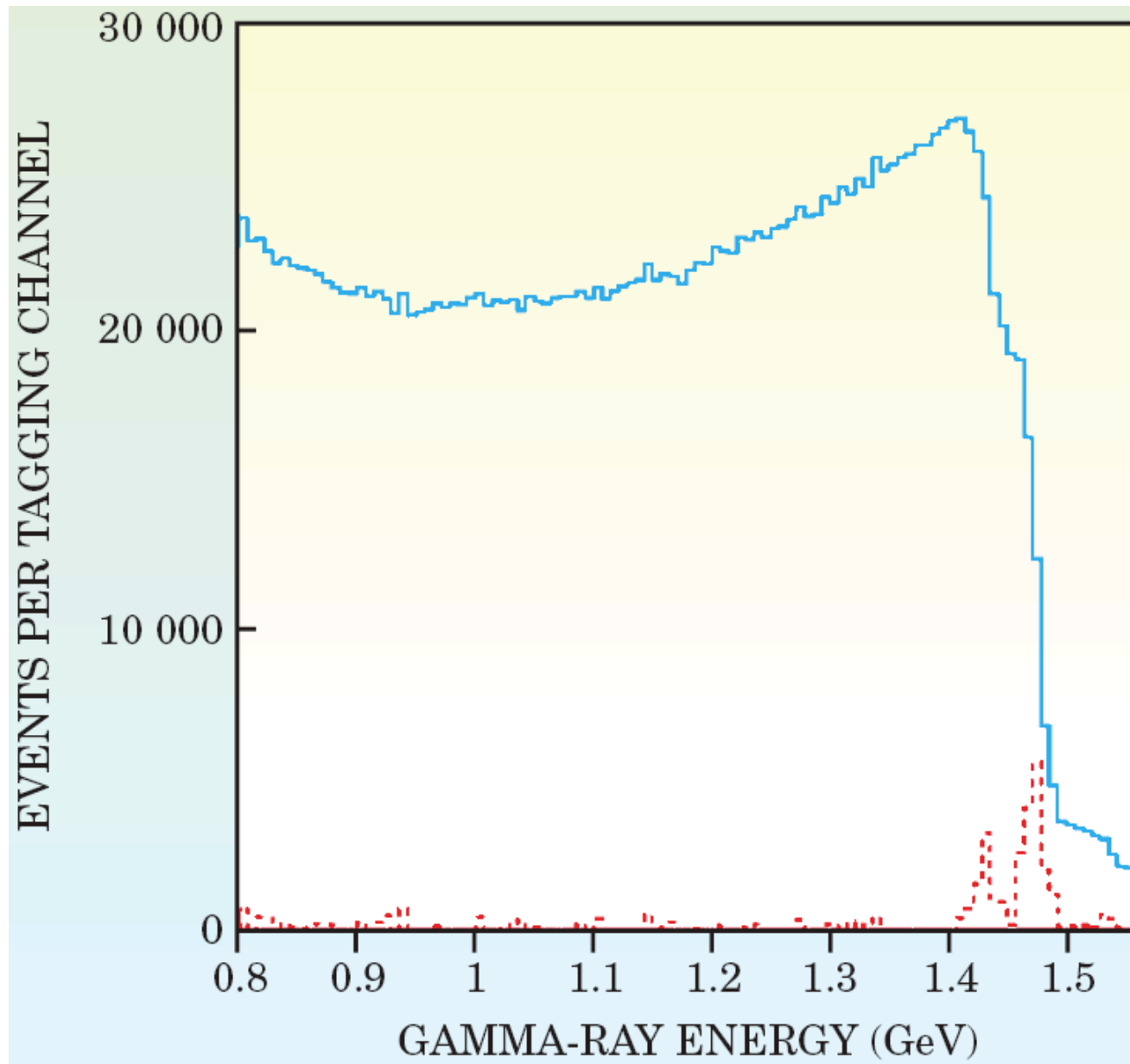
Work in progress

$$\vec{\gamma} + n \rightarrow \pi^0 + n$$

$$\vec{\gamma} + p \rightarrow \omega + p$$

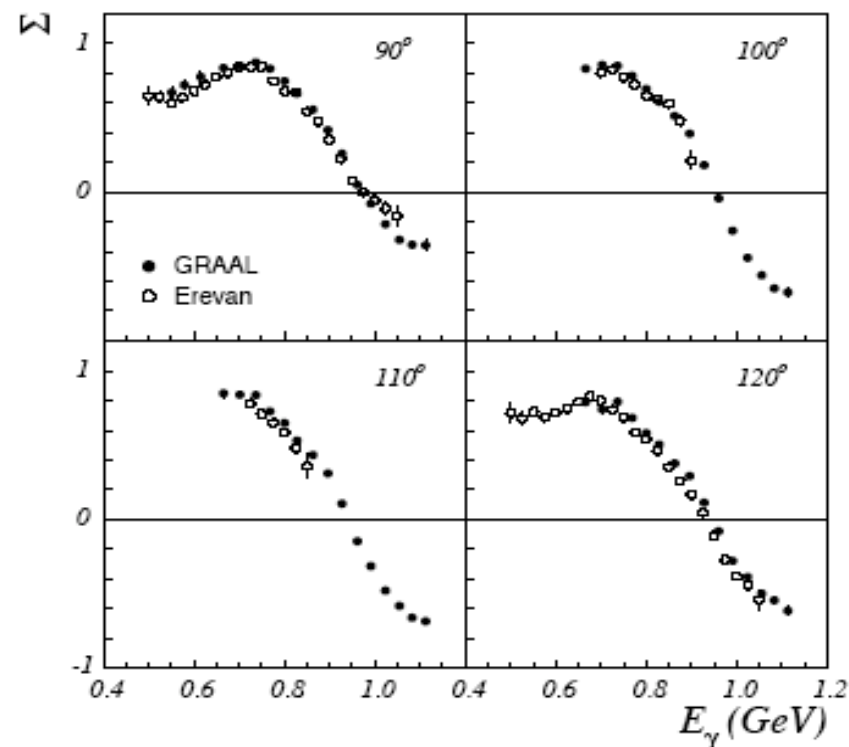
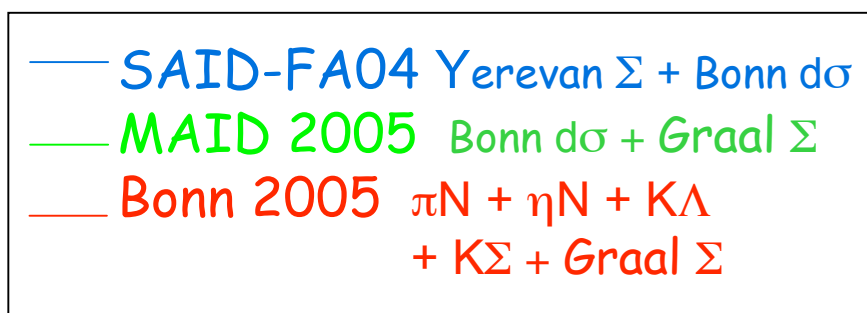
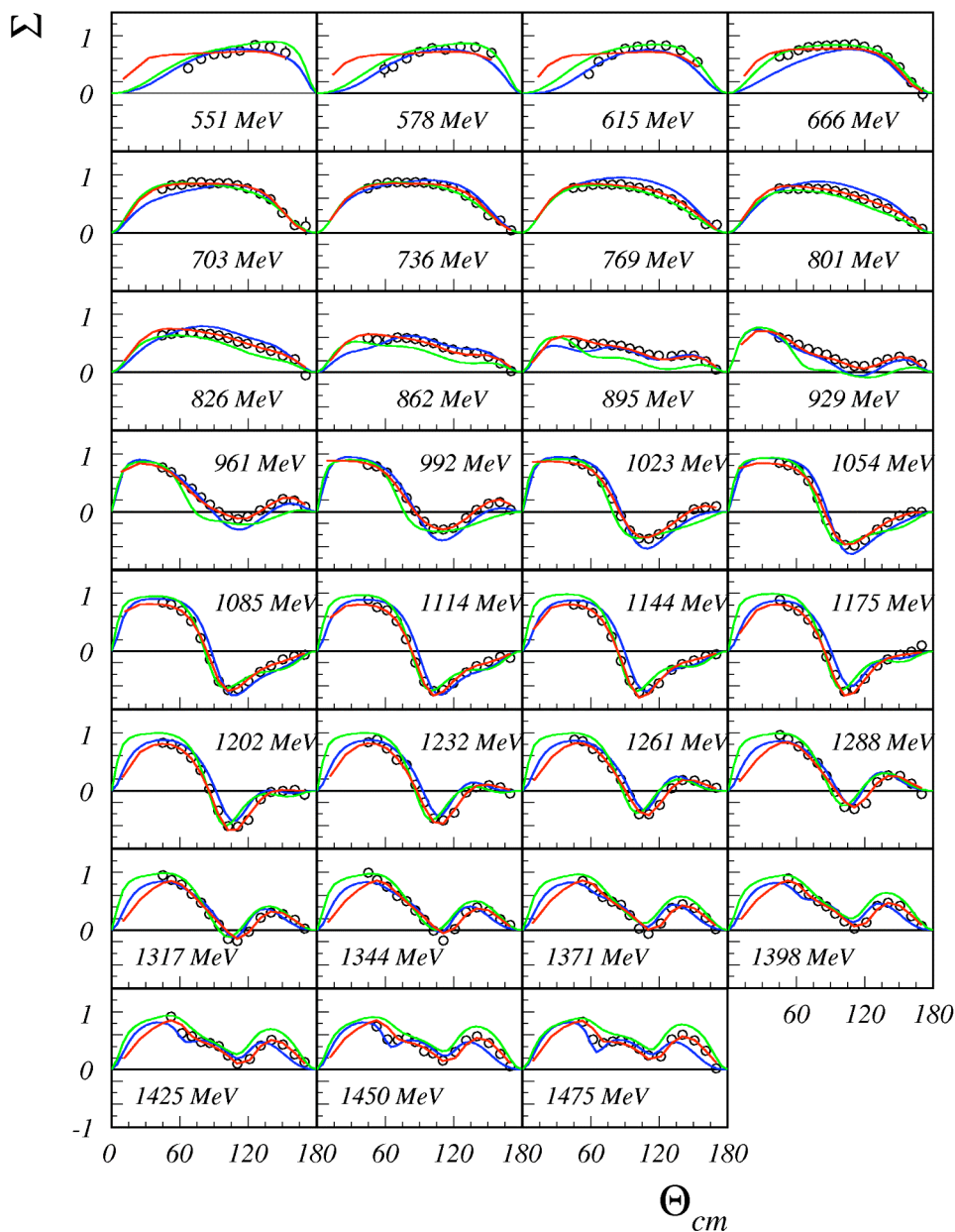
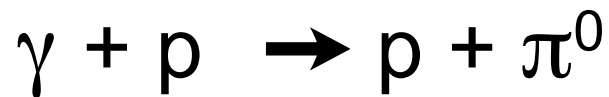
$$\vec{\gamma} + d \rightarrow p + n$$

# Gamma-ray Energy Spectrum of Ladon Beams



Graal beam with  
3 UV laser lines

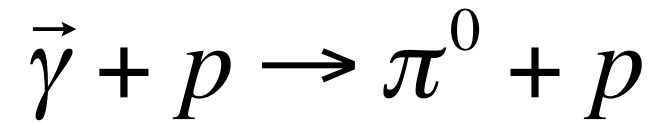
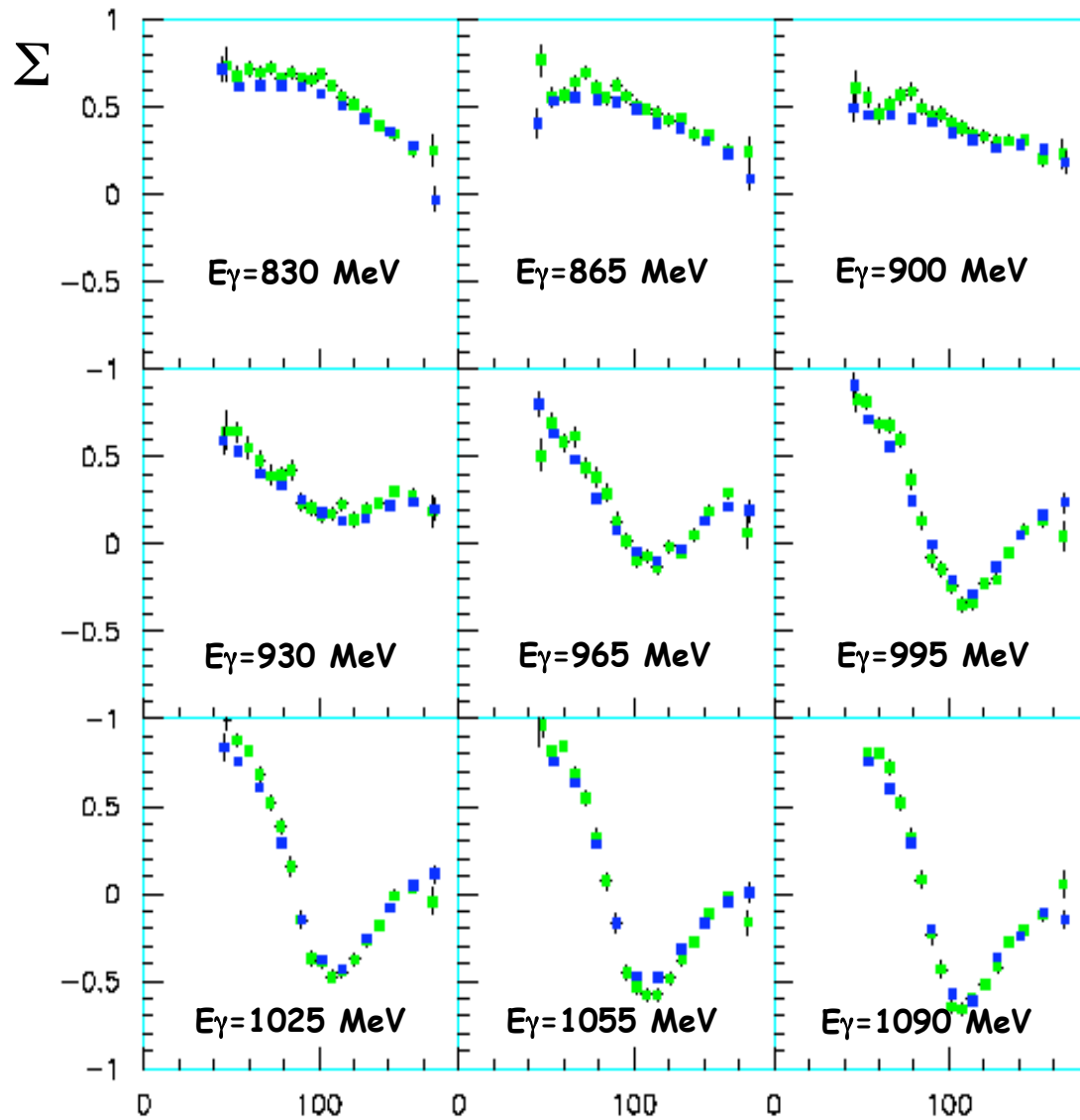
# Asimmetry $\Sigma$



• Graal    ◦ Yerevan



# Comparison of asymmetry results obtained with the Green and UV

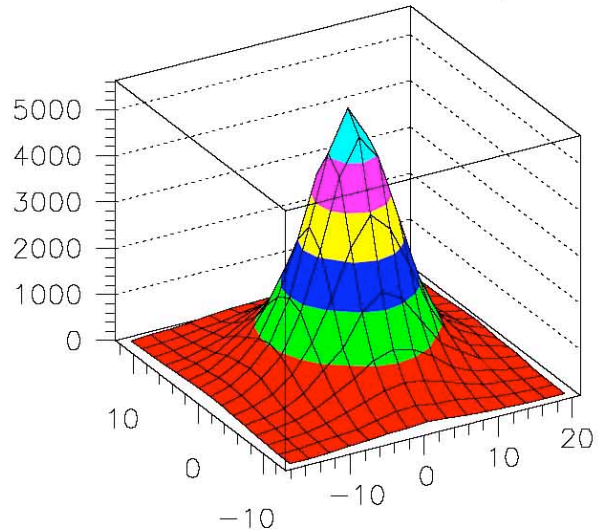


Different laser lines produce gamma-ray beams of different intensities and polarization at the same gamma-ray energy.

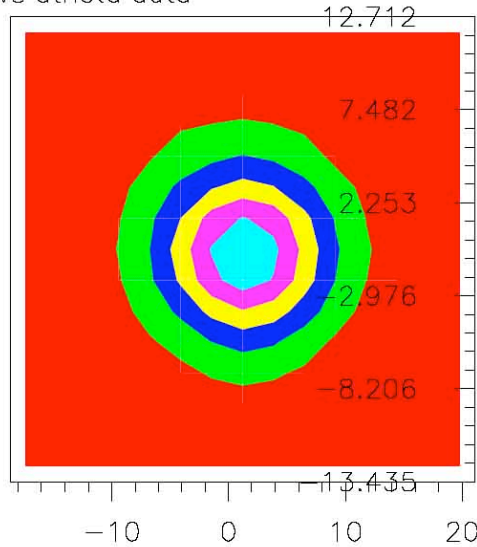
 $\theta_{\pi^0}^{\text{CM}}$



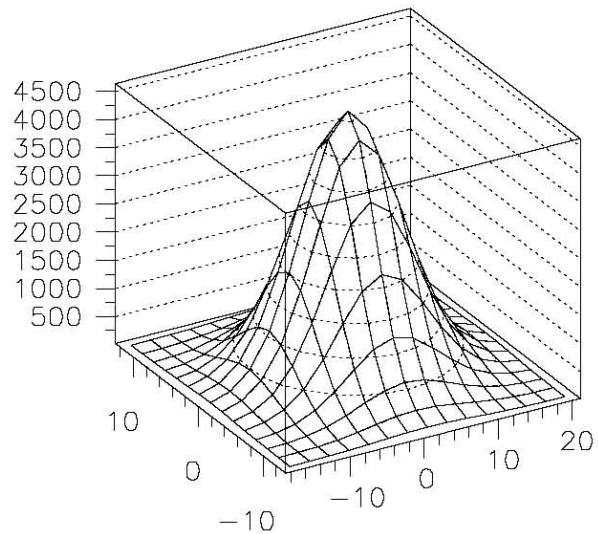
central proton coplan vs dtheta data



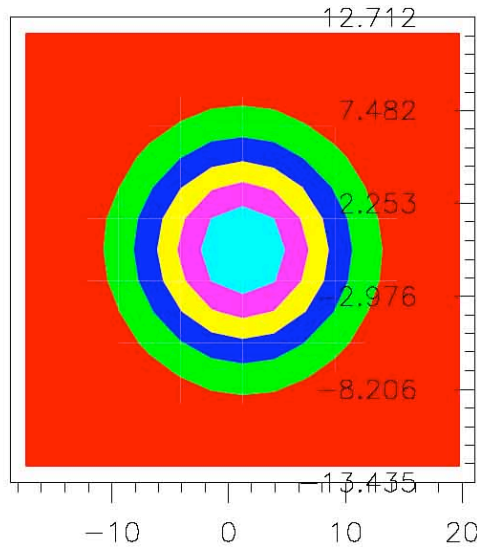
deltatheta vs coplanarity



deltatheta vs coplanarity



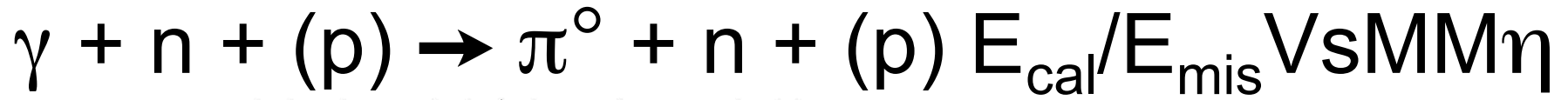
fitzfunz2006.f



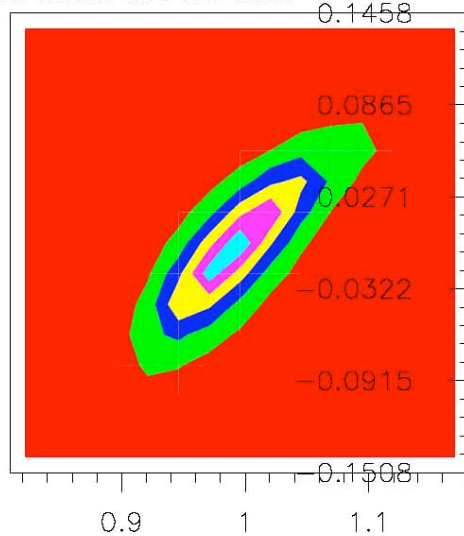
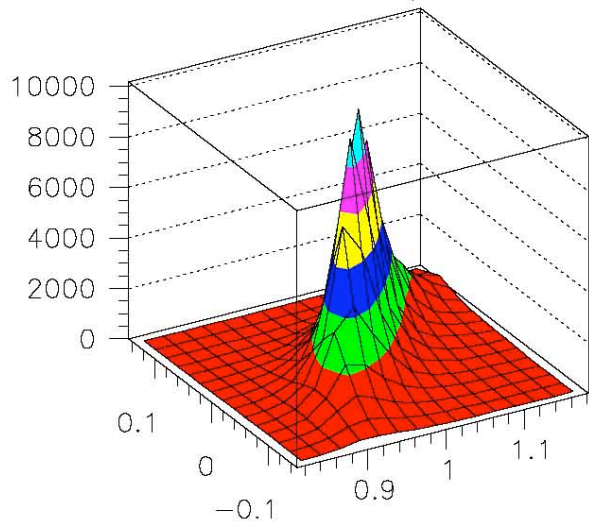
fitzfunz2006.f

Monday, May 26, 2008

ICTP May 14, 2008

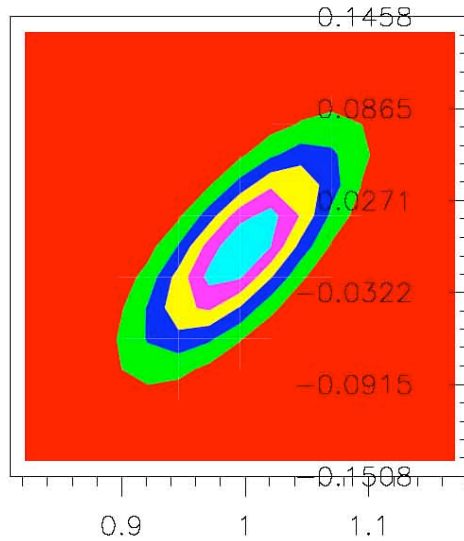
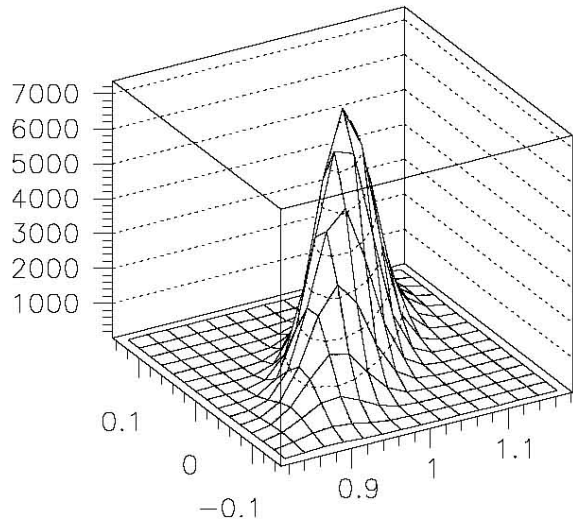


central proton ecalceta/eeta vs missmass eta data



rmiss from eta vs ecalc eta/emeas eta

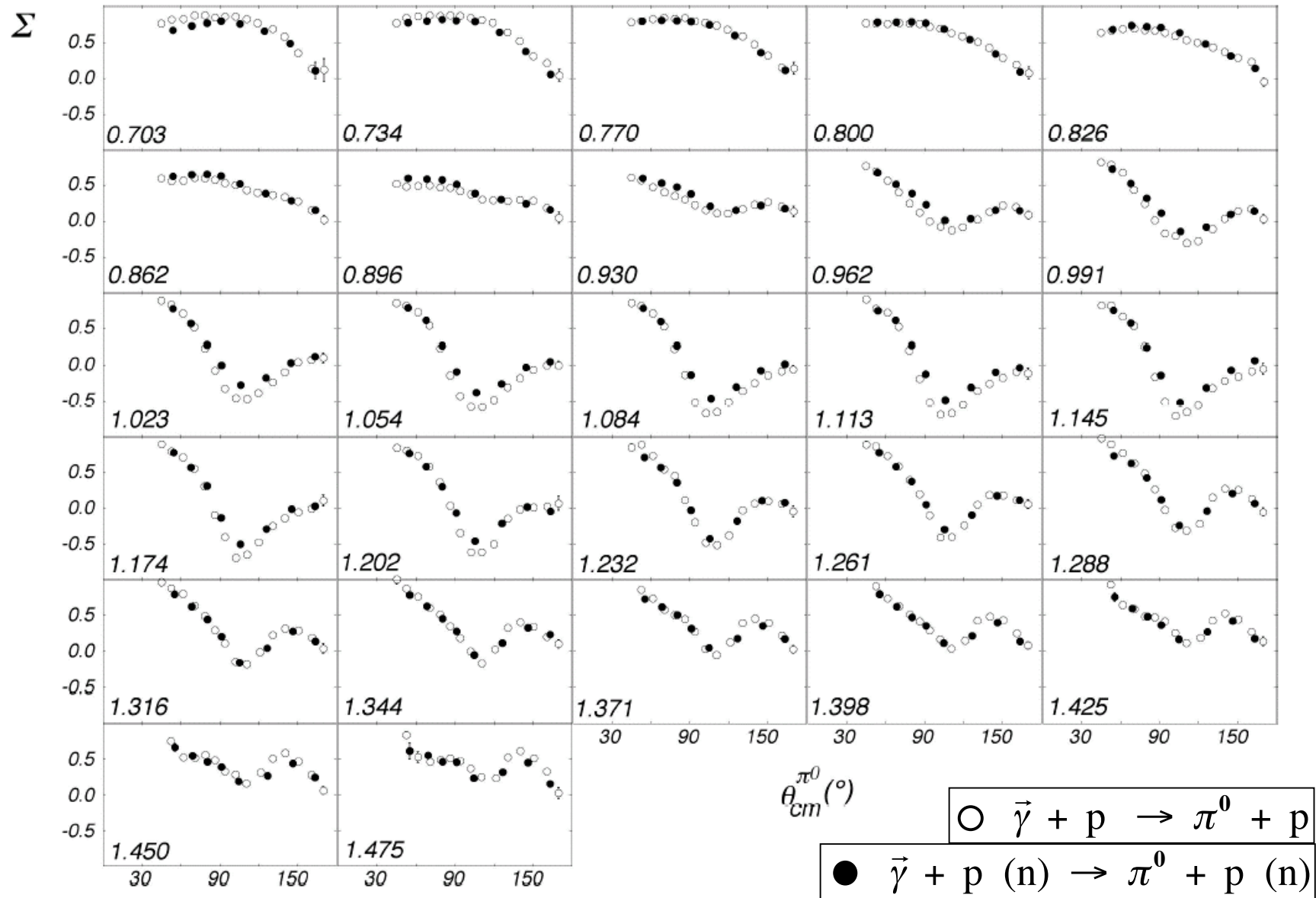
rmiss from eta vs ecalc eta/emeas eta

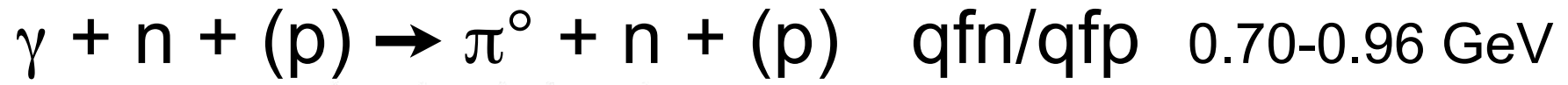


fitzfunz2006.f

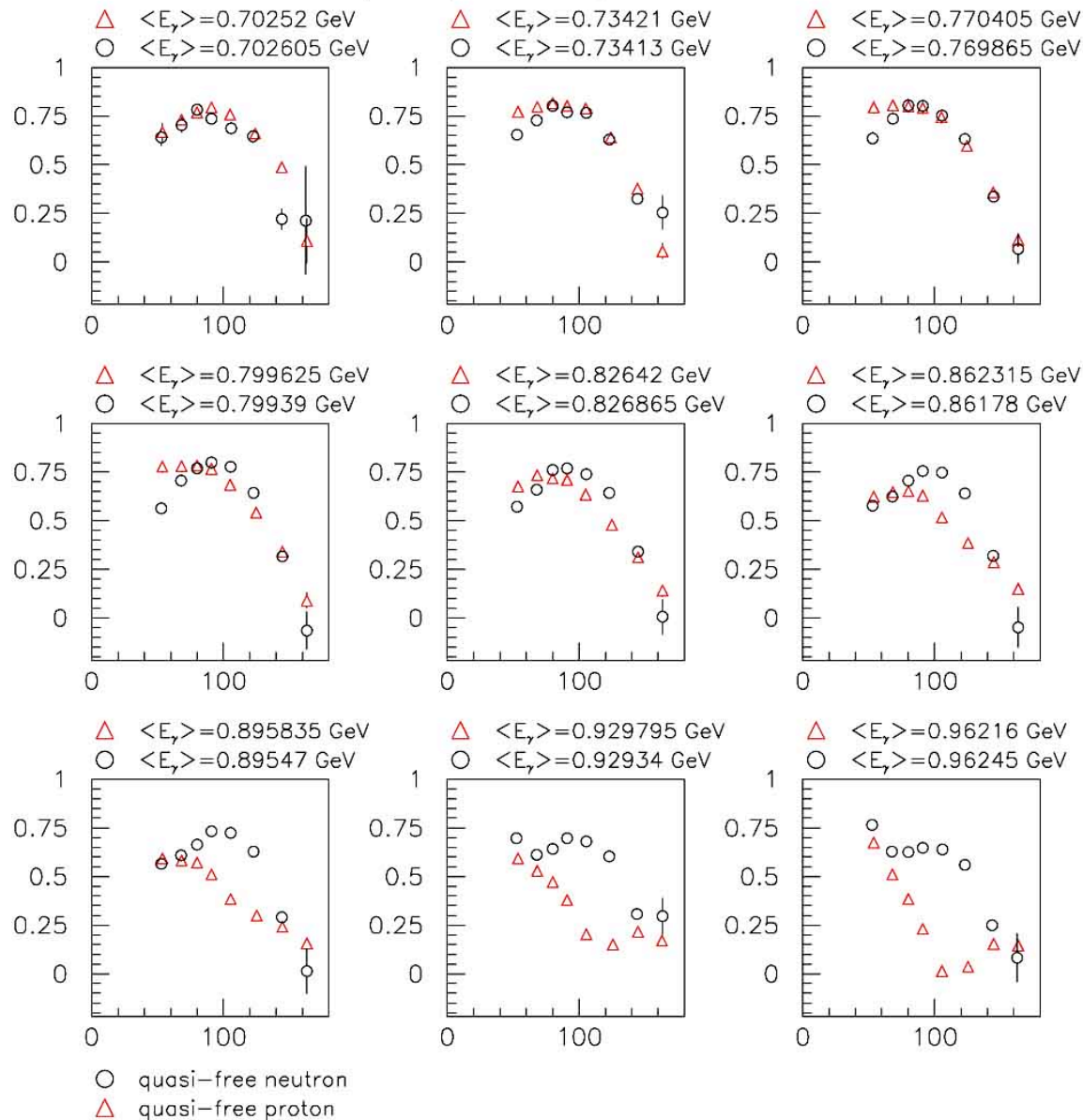
fitzfunz2006.f

# $\gamma + p + (n) \rightarrow \pi^0 + p + (n)$ fp vs qfp

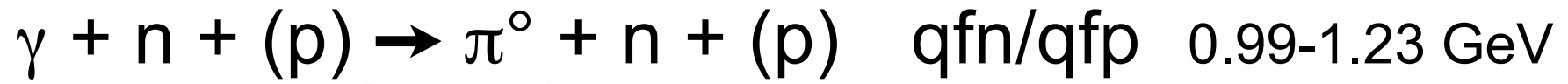




q-free proton and q-free neutron

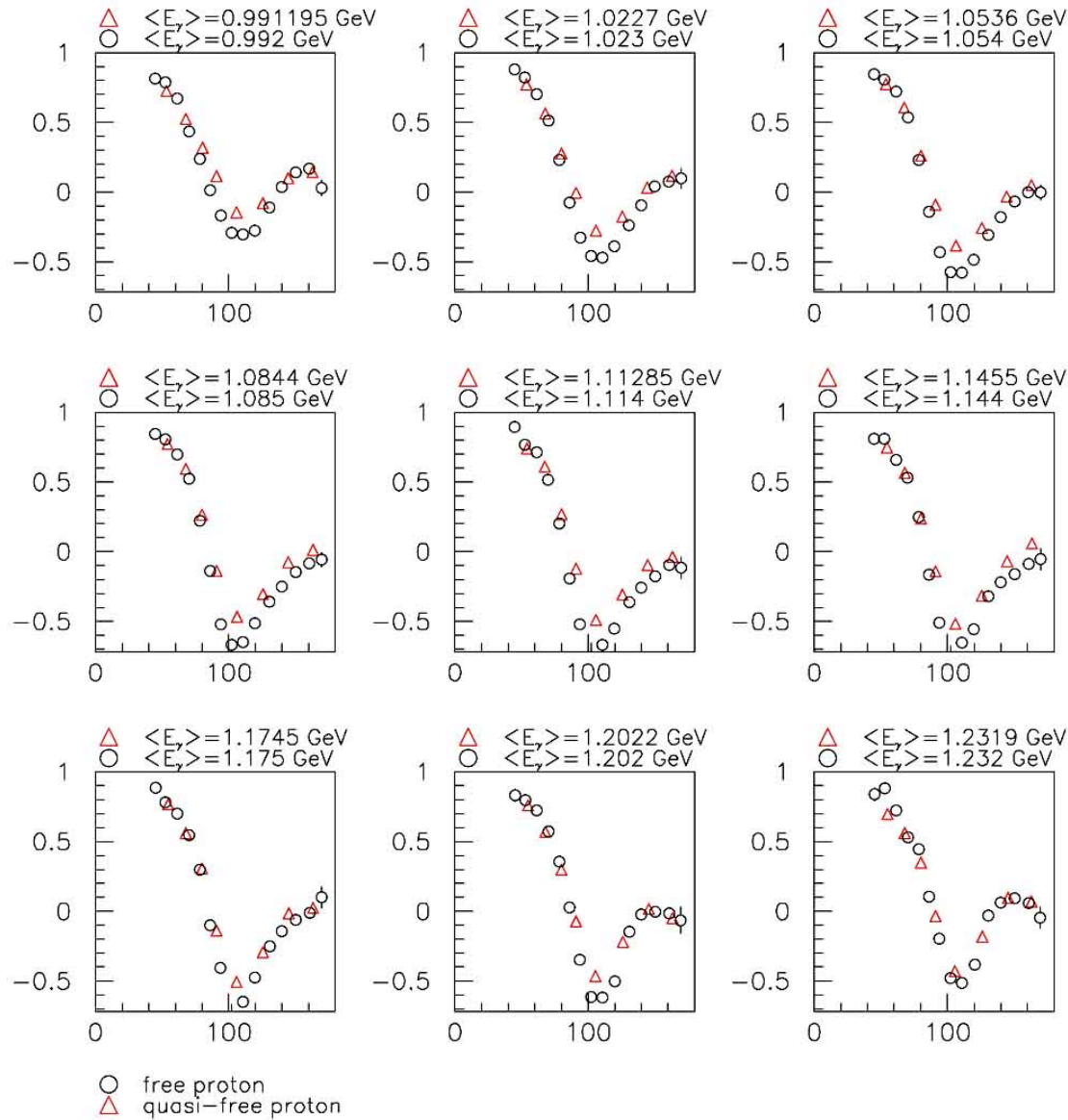


$\pi^0$  asymmetries  
 quasi-free proton  
 VS  
 quasi-free neutron  
 0.70-0.96 GeV



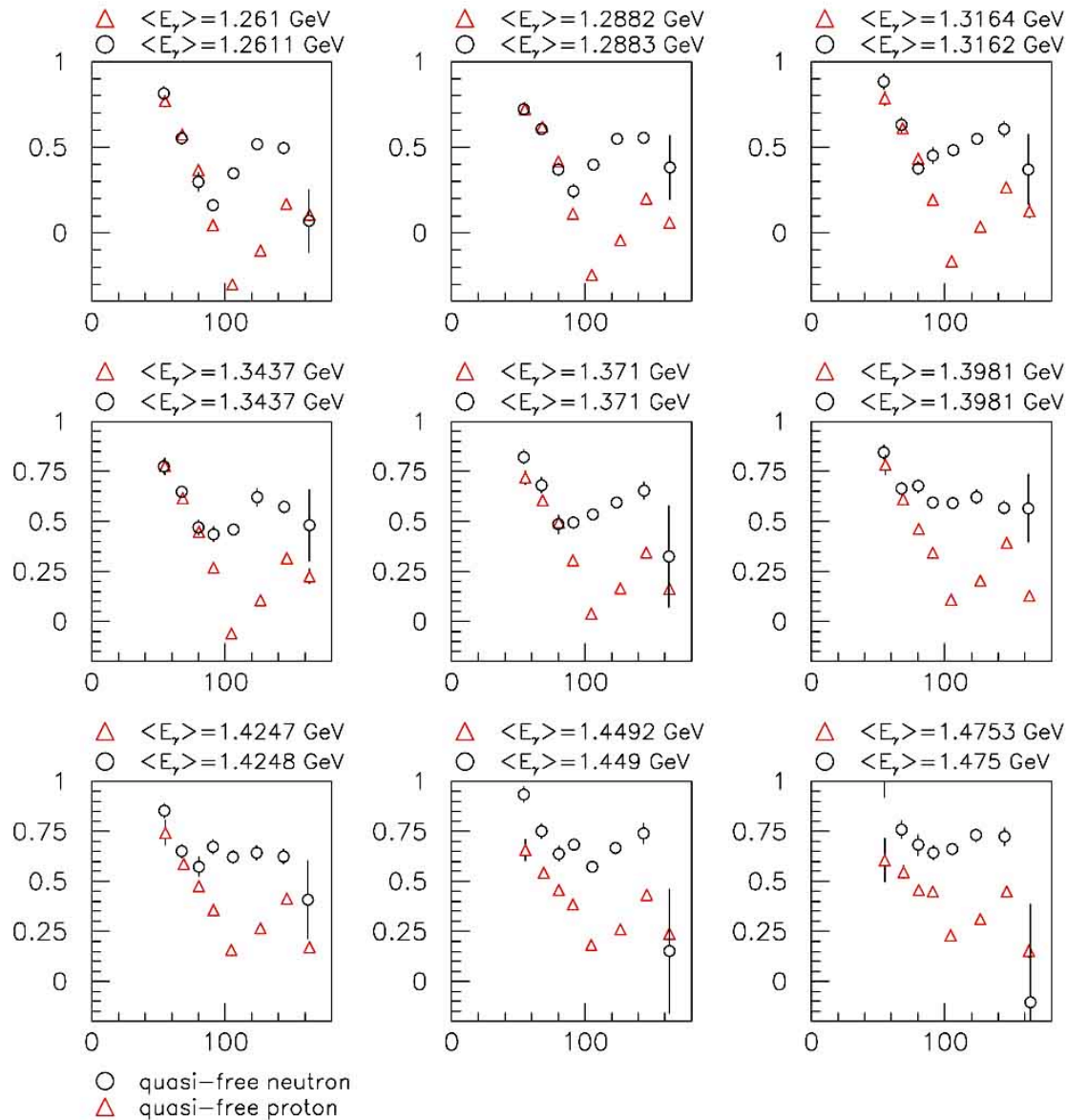
q-free proton and free proton

$\pi^0$  asymmetries  
quasi-free proton  
vs  
quasi-free neutron  
0.99-1.23 GeV



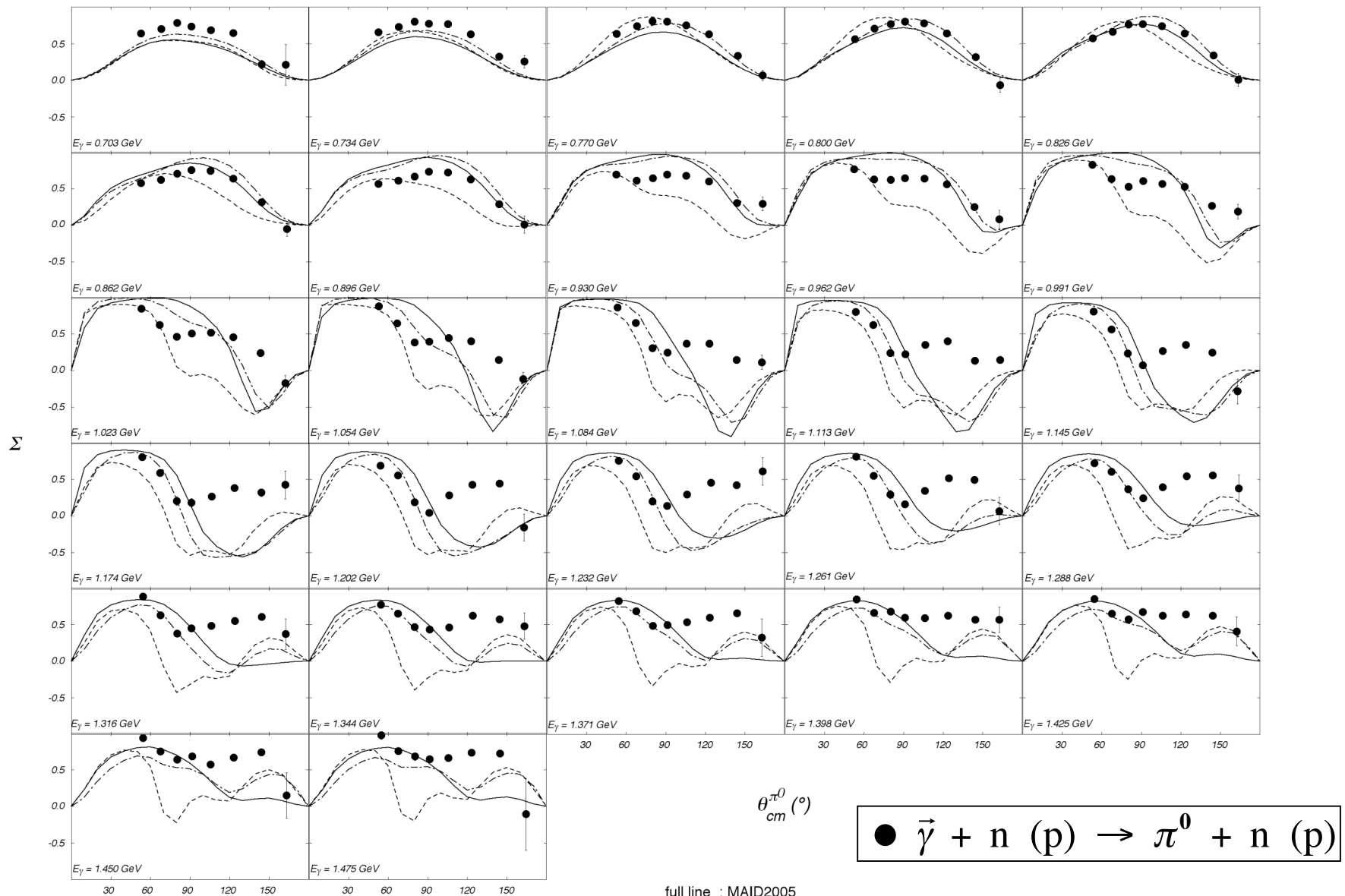
# $\gamma + n + (p) \rightarrow \pi^0 + n + (p)$ qfn/qfp 1.26-1.47 GeV

q-free proton and q-free neutron



$\pi^0$  asymmetries  
 quasi-free proton  
 vs  
 quasi-free neutron  
 1.26-1.47 GeV

# $\gamma + n + (p) \rightarrow \pi^0 + n + (p)$ quasi-free n





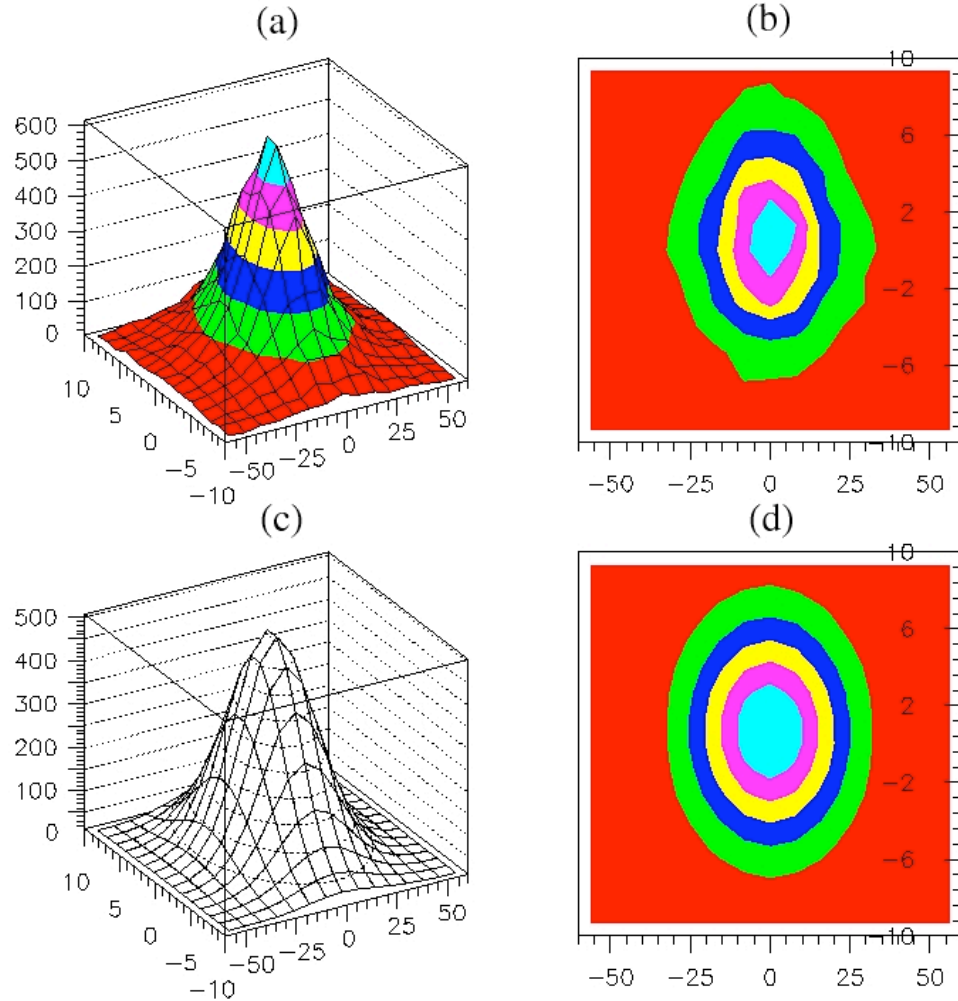
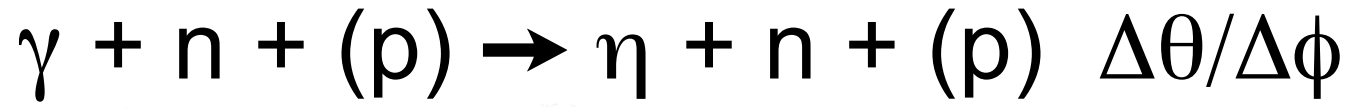


FIG. 1: Upper part: The correlation  $\Delta\theta$  vs.  $(\Delta\phi - 180^\circ)$  in three-dimensional view(a) and its projection on two dimensions (b); Lower part: The bidimensional gaussian fit (c) and its projection on two dimensions (d).

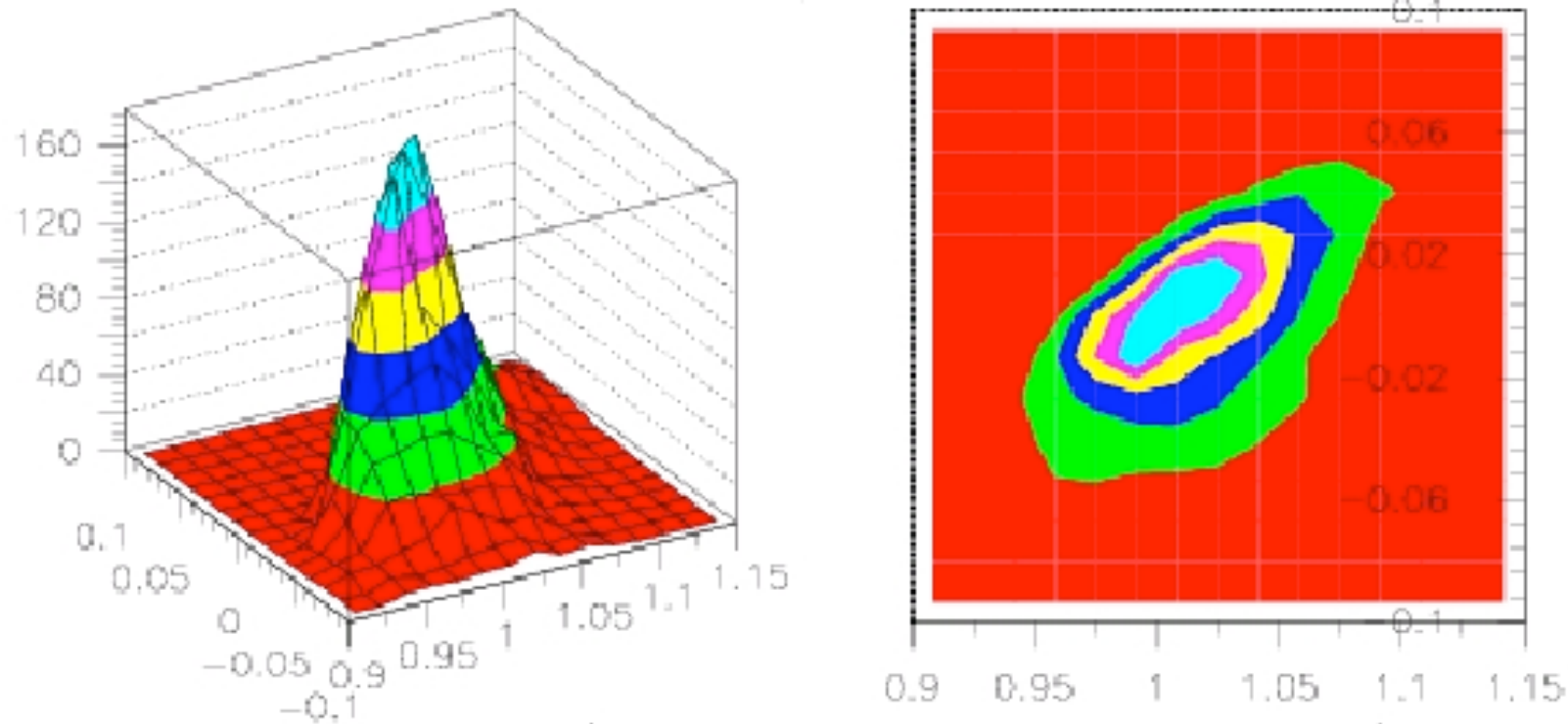
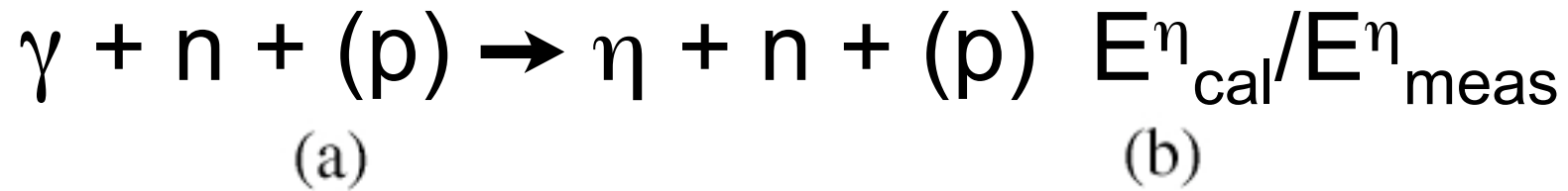


FIG. 2: The three-dimensional correlation  $E_{\eta}^{\text{calc}}/E_{\eta}^{\text{meas}}$  vs.  $(M_X - M_N)$  (a) (see text for explanation) and its projection on two dimensions (b).

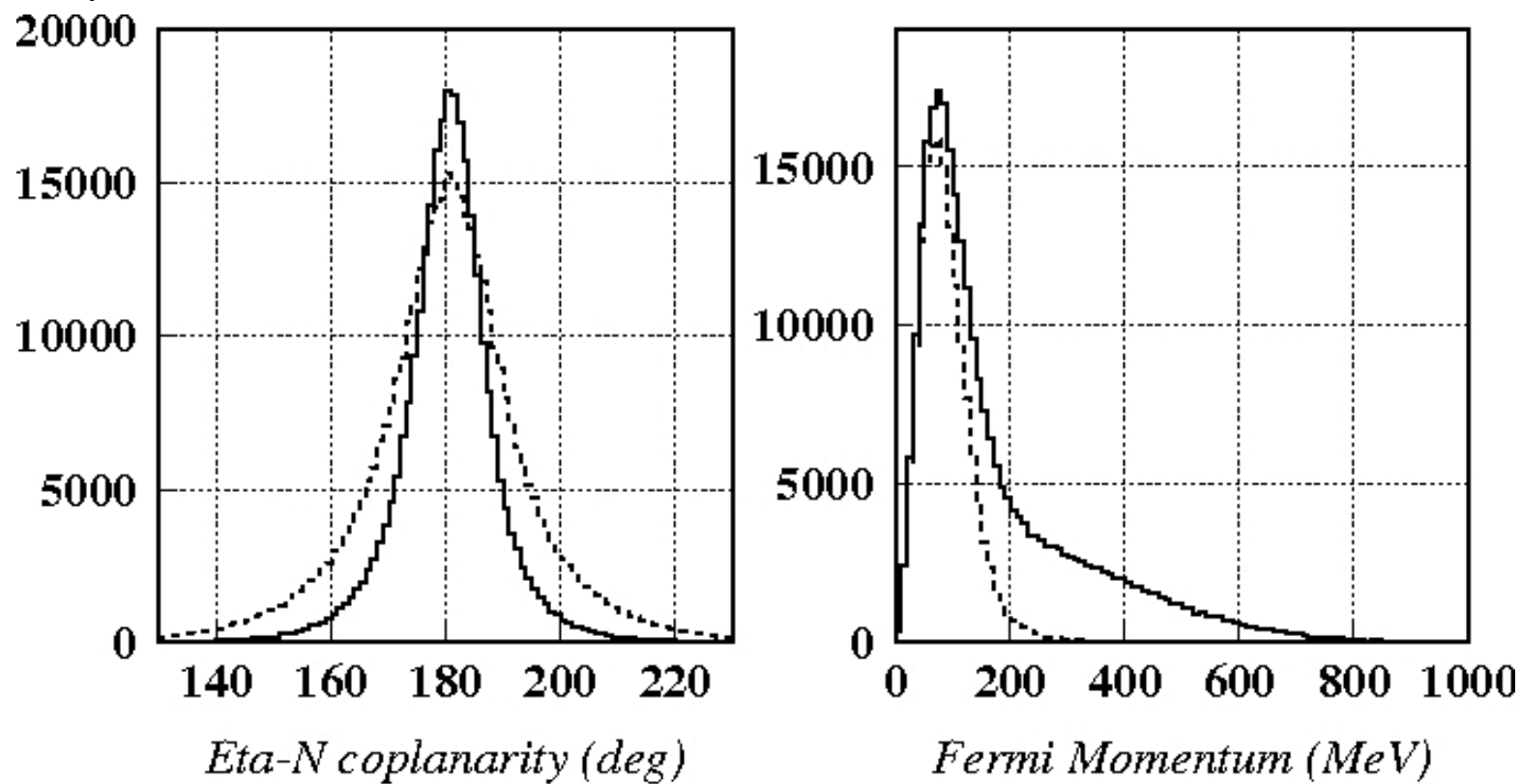
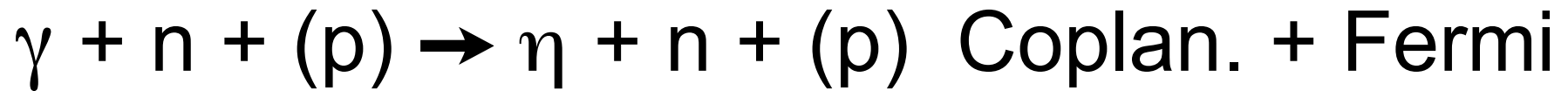
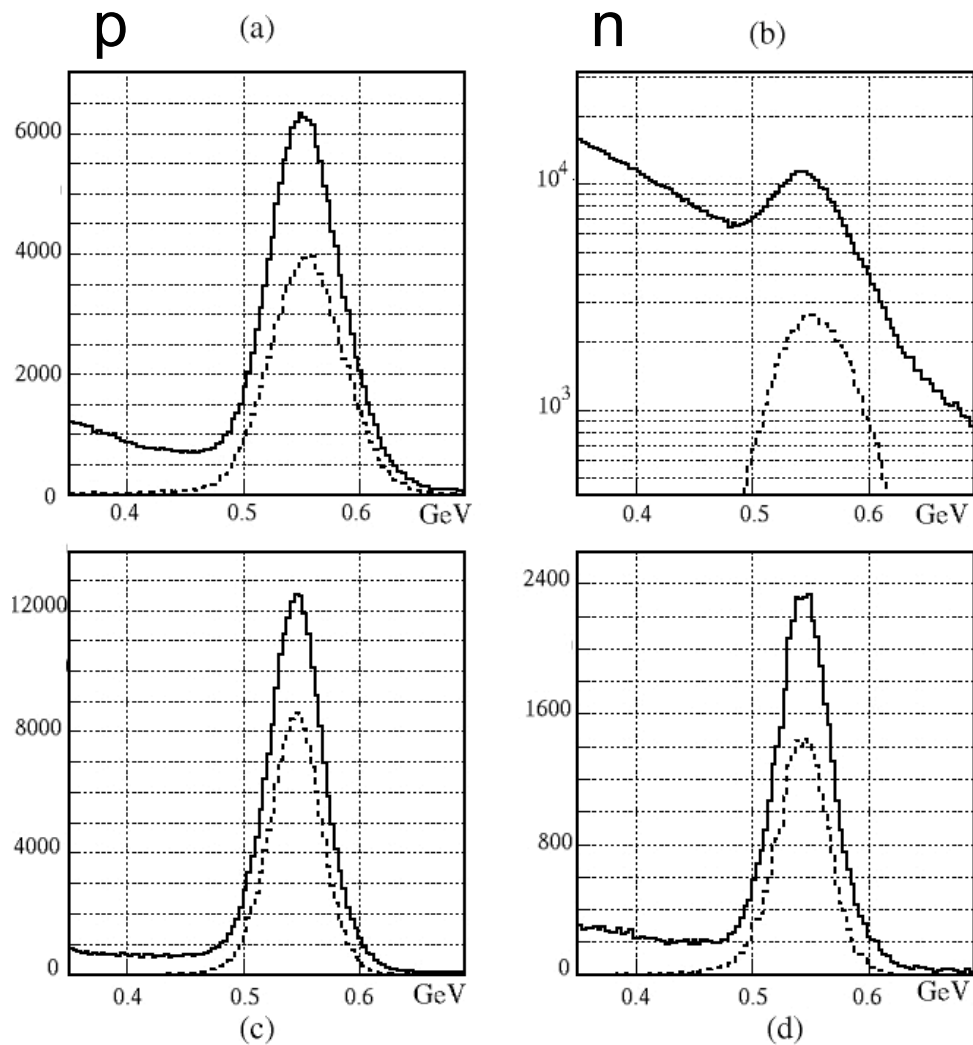


FIG. 5: Left: Coplanarity between the  $\eta$  and the free proton (solid line) and the quasi-free proton (dotted line): the smearing between the two distributions is due to the Fermi motion; Right: The Fermi momentum distribution before (solid line) and after (dashed line) the application of the bidimensional cuts (see text for details).

# $\gamma + n + (p) \rightarrow \eta + n + (p)$ Invariant Mass



Nucleon in BGO

Nucleon forward

FIG. 3: The  $\eta$  invariant mass without cuts (solid line) and with the kinematical cuts (dotted line) for a central proton (a) and neutron (b) (in logarithmic scale), for a forward proton (c) and neutron (d).

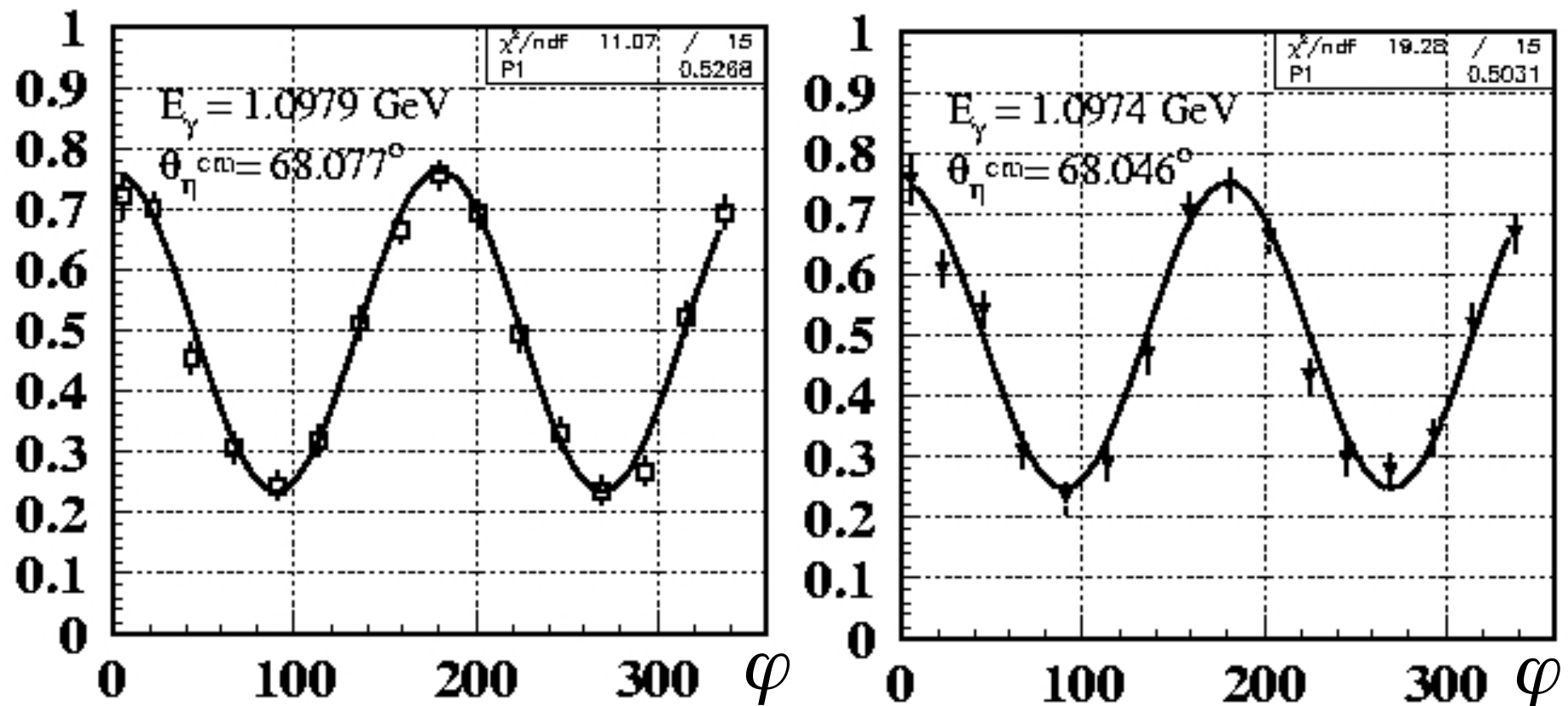


FIG. 4: The azimuthal distribution of the ratio (2) for the q.f. proton (a) and q.f. neutron (b) data in a fixed bin of  $E_\gamma$  and  $\theta_\eta^{cm}$ .

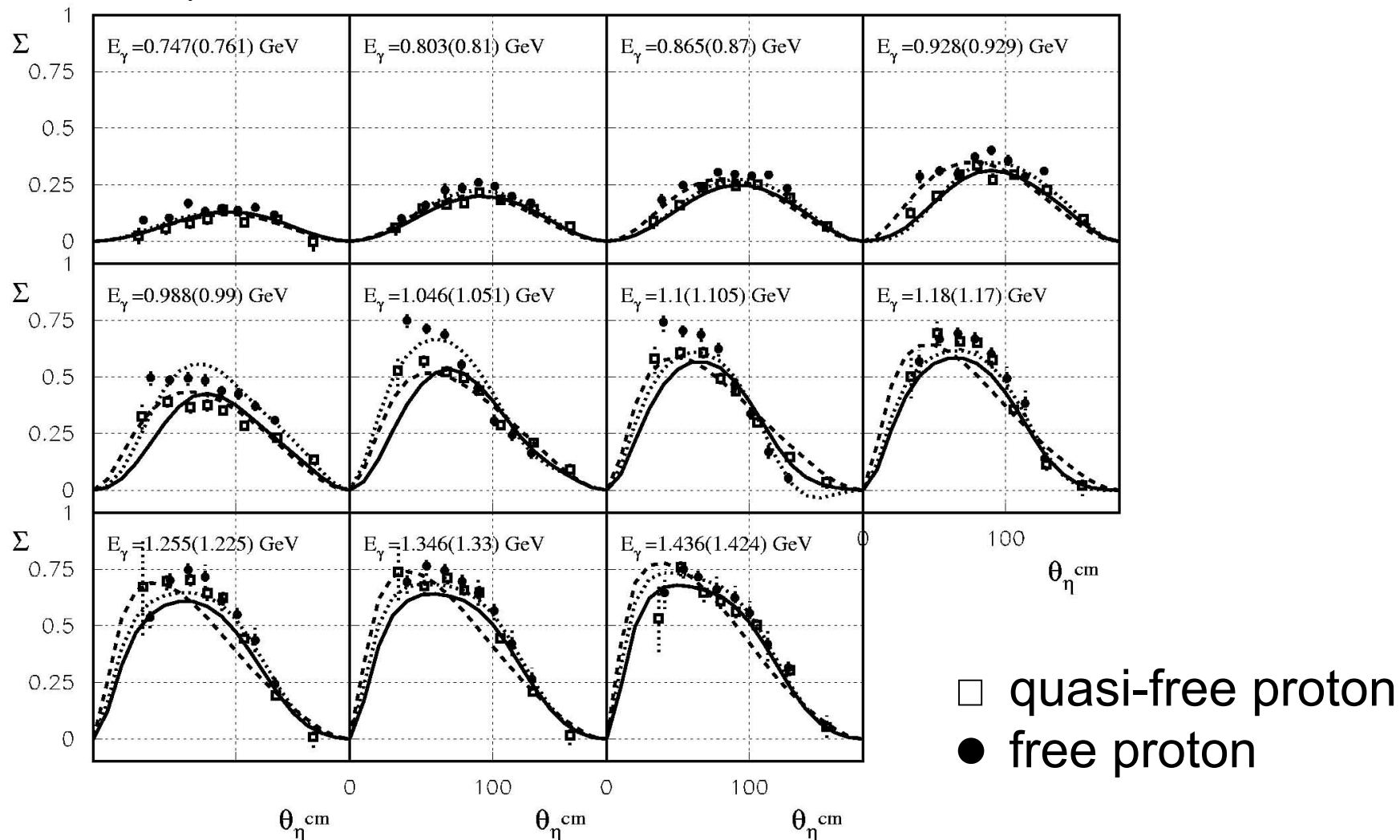


FIG. 6: Beam asymmetry  $\Sigma$  in  $\eta$  photoproduction on the quasi-free proton (open squares) in the deuteron and on the free proton (full circles)[2]. The energy value outside and inside parenthesis indicate the mean value of the bin for quasi free and free protons respectively. In dotted lines are illustrated the predictions of Maid2001 [7] for the free proton, in solid and dashed lines those for the quasi-free proton of Maid2001 [7] and the reggeized model [3], respectively (see text for details).

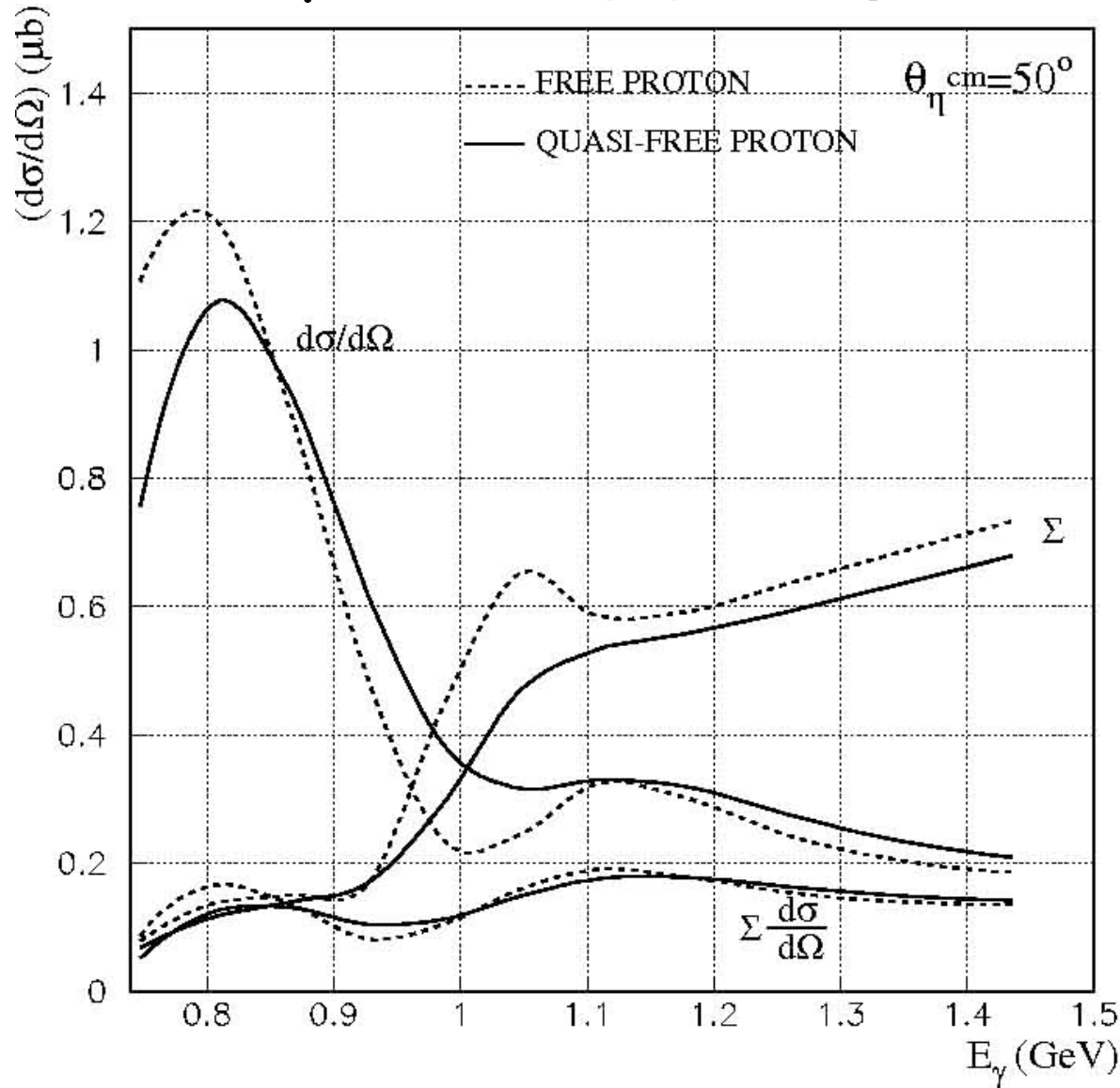
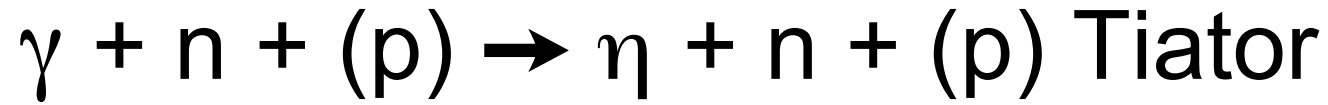


FIG. 7: Energy dependence of the differential cross section for  $\gamma p \rightarrow \eta p$  calculated at  $\theta = 50^{\circ}$ . The unpolarized cross section (5), the polarized cross section (6) and the beam asymmetry  $\Sigma$  are presented in the three pairs of curves for the free proton (dashed curves) and the quasi free proton (solid curves) respectively.

# $\gamma + n + (p) \rightarrow \eta + n + (p) \quad \Sigma(\theta) \text{ qfn}$

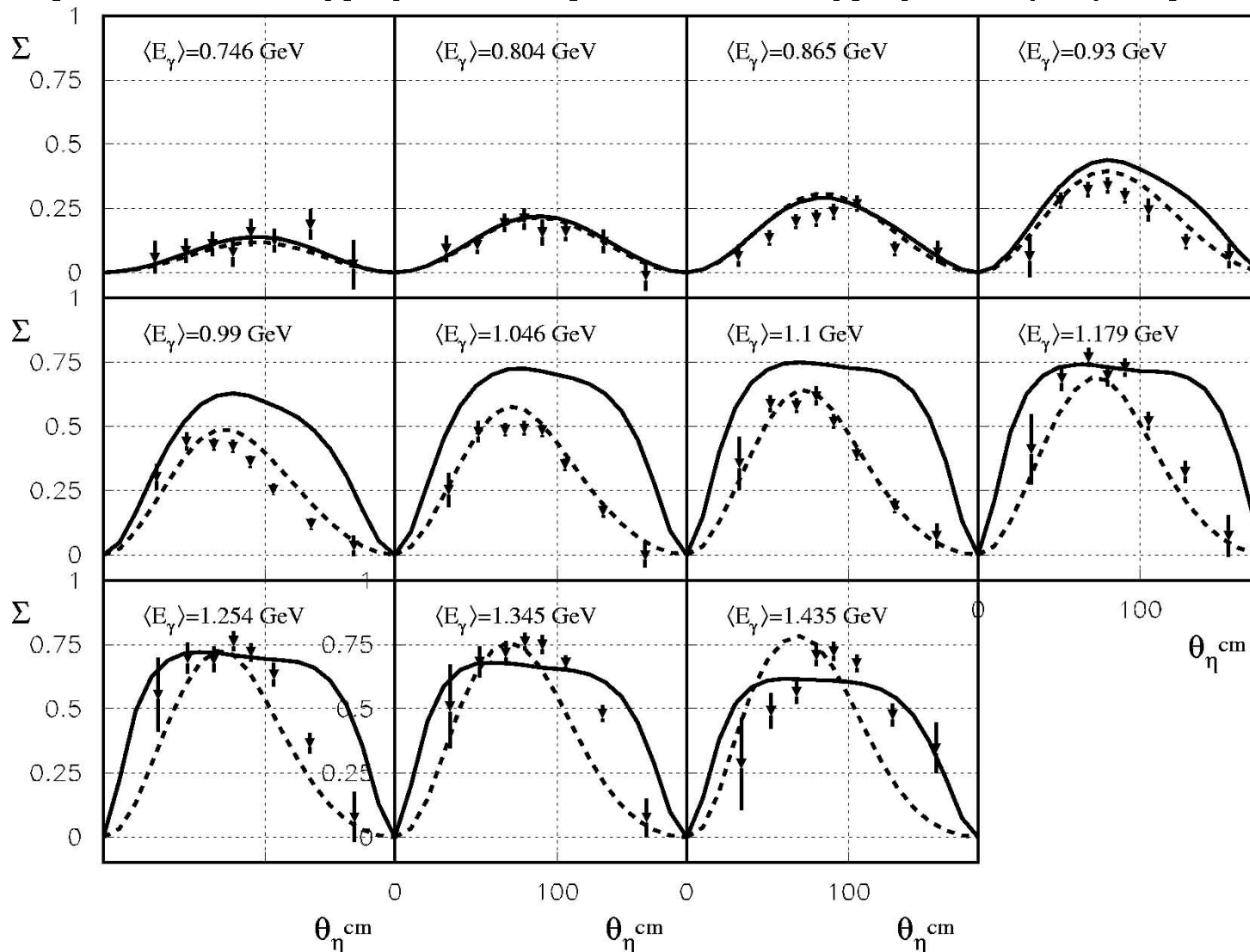


FIG. 8: Beam asymmetry  $\Sigma$  in  $\eta$  photoproduction on the quasi-free neutron in eleven energy bins, plotted as a function of the  $\theta_{\eta}^{cm}$ . In each plot, the mean  $\gamma$  energy of the bin is also indicated. In solid and dashed lines are illustrated the predictions for neutrons of Maid2001 and of the reggeized model respectively (see text for details).



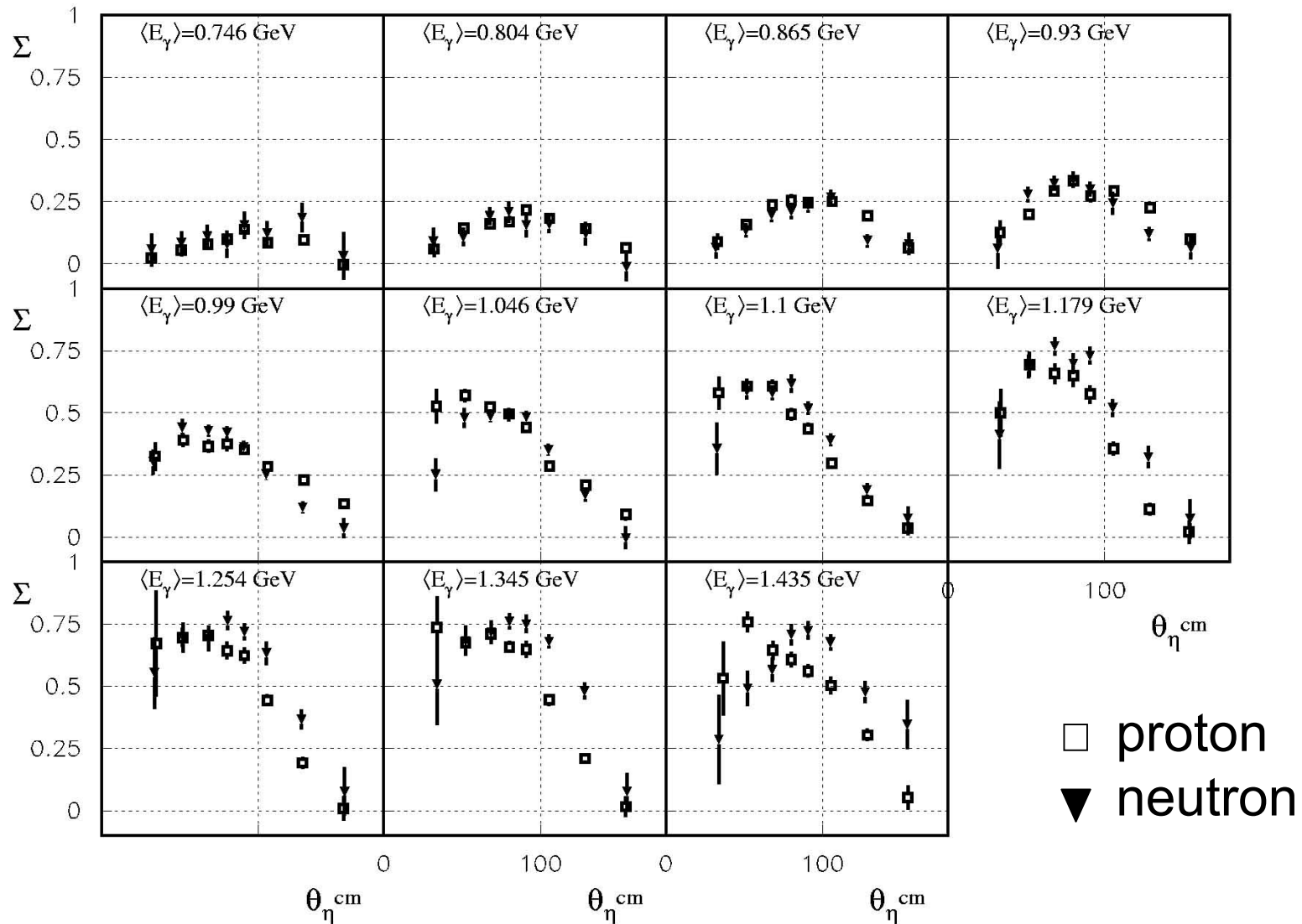
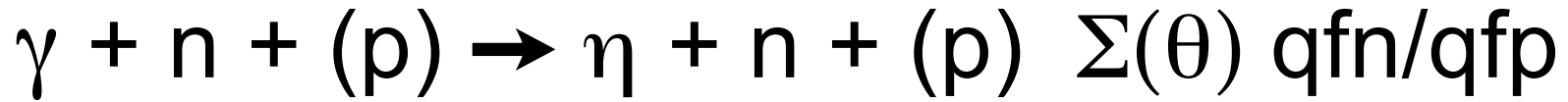
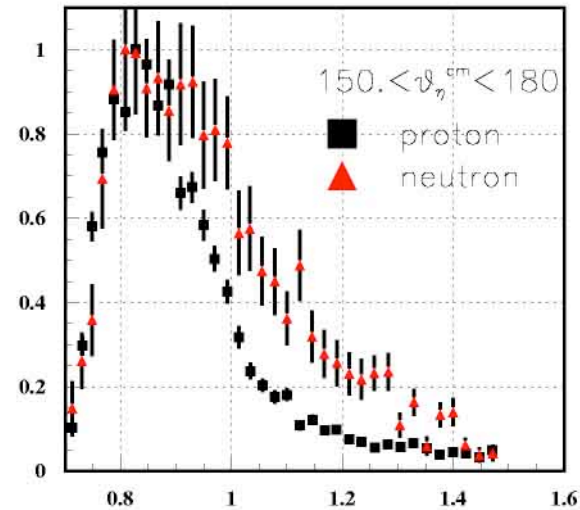
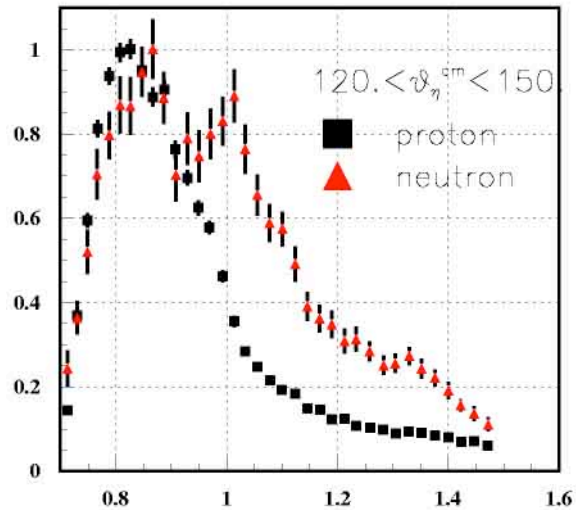
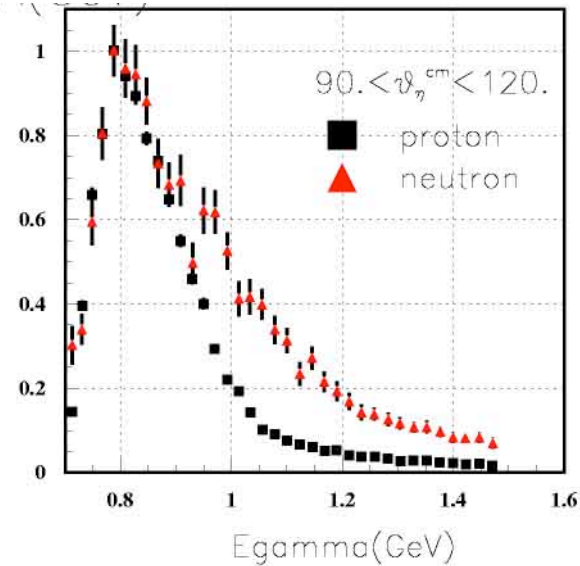
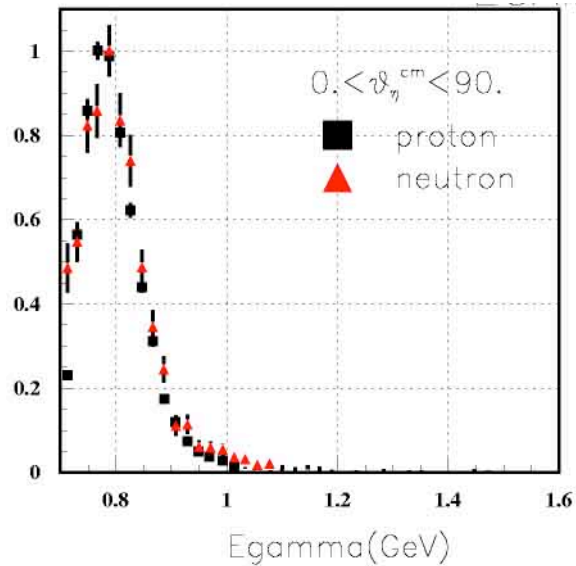


FIG. 9: Comparison between the beam asymmetry  $\Sigma$  in  $\eta$  photoproduction on the quasi-free proton (open squares) and the quasi-free neutron (full triangles) in the eleven energy bins, plotted as a function of the  $\theta_{\eta}^{cm}$ . See text for details.

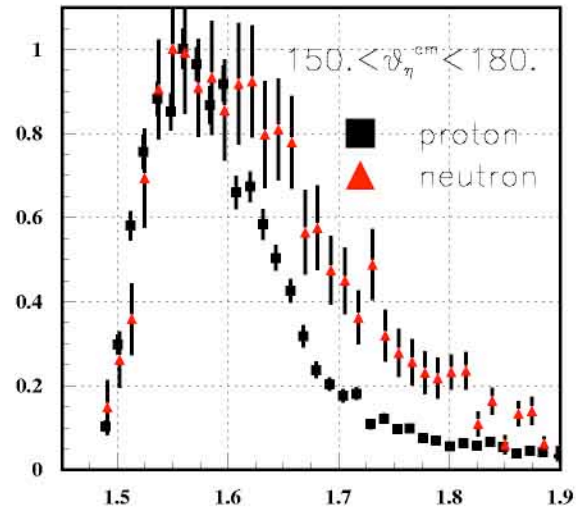
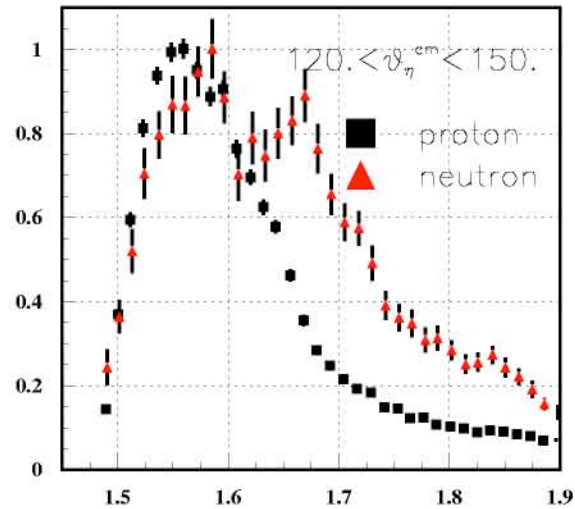
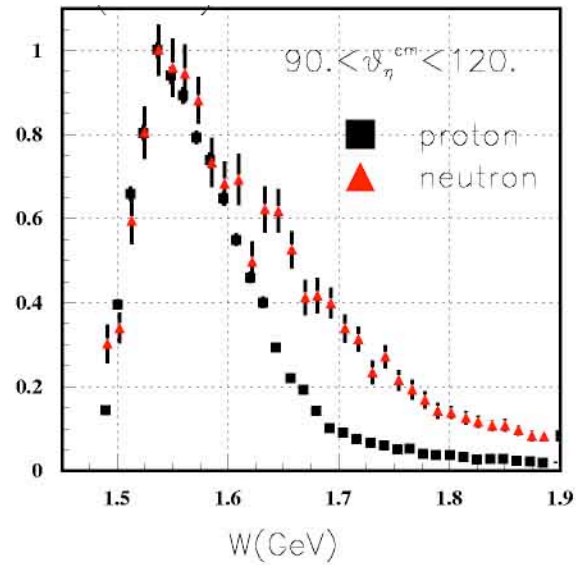
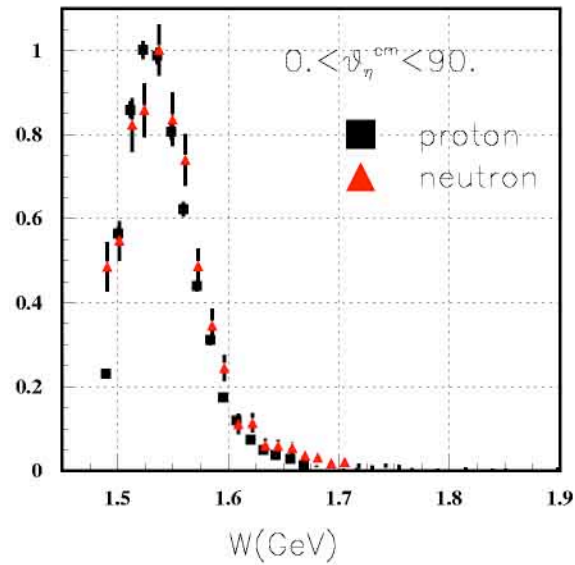
# $\gamma + n + (p) \rightarrow \eta + n + (p)$ Yield( $E_\gamma$ )



Monday, May 26, 2008

ICTP May 14, 2008

# $\gamma + n + (p) \rightarrow \eta + n + (p)$ Yield(W)



Monday, May 26, 2008

ICTP May 14, 2008

27

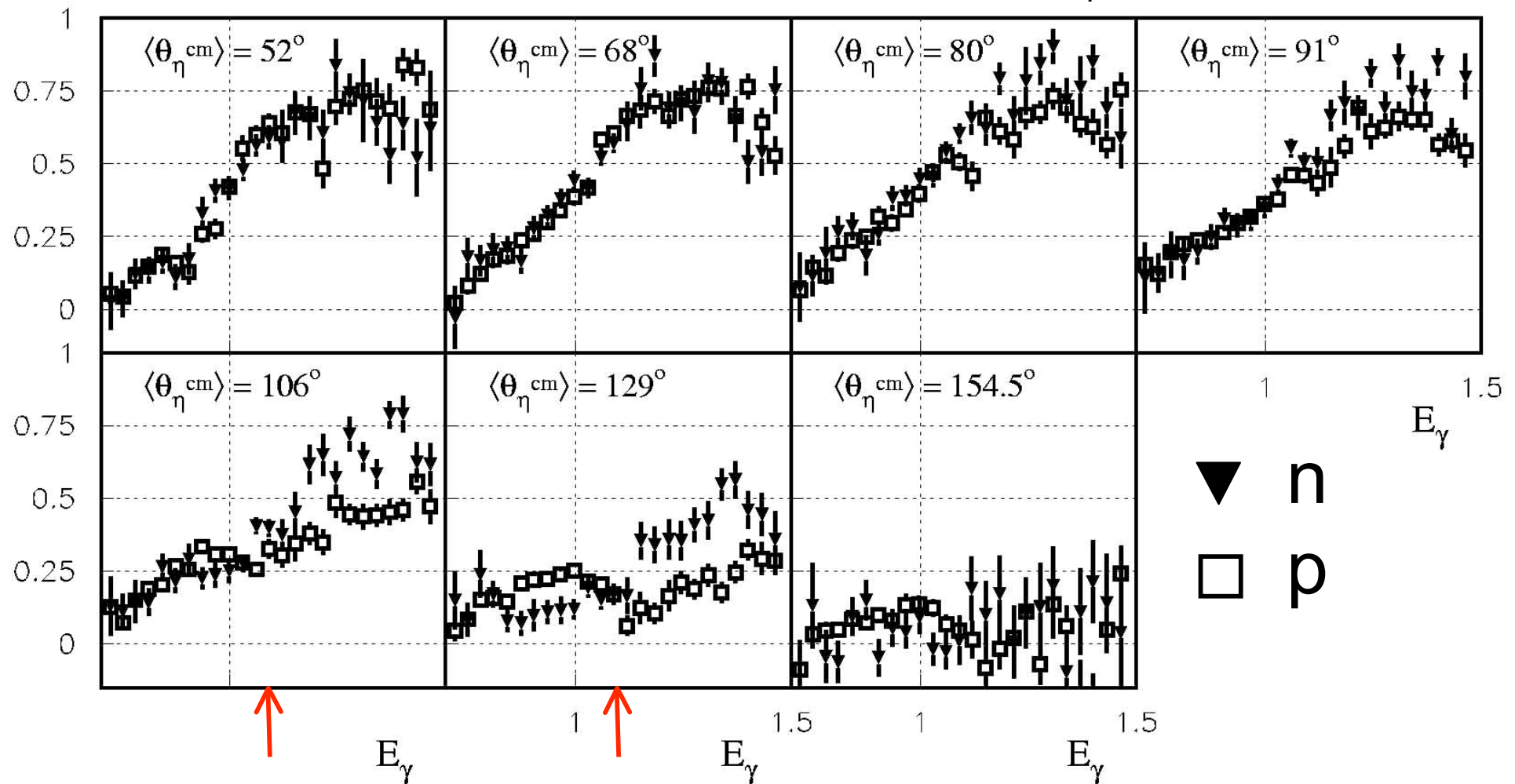
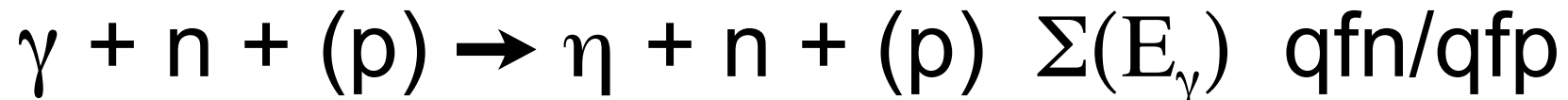


FIG. 10: Comparison between the beam asymmetry  $\Sigma$  in  $\eta$  photoproduction on the quasi-free proton (open squares) and the quasi-free neutron (full triangles) in seven angular bins, plotted as a function of the  $\gamma$  energy (intervals of  $\simeq 25$  MeV width).

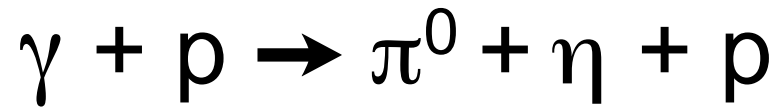
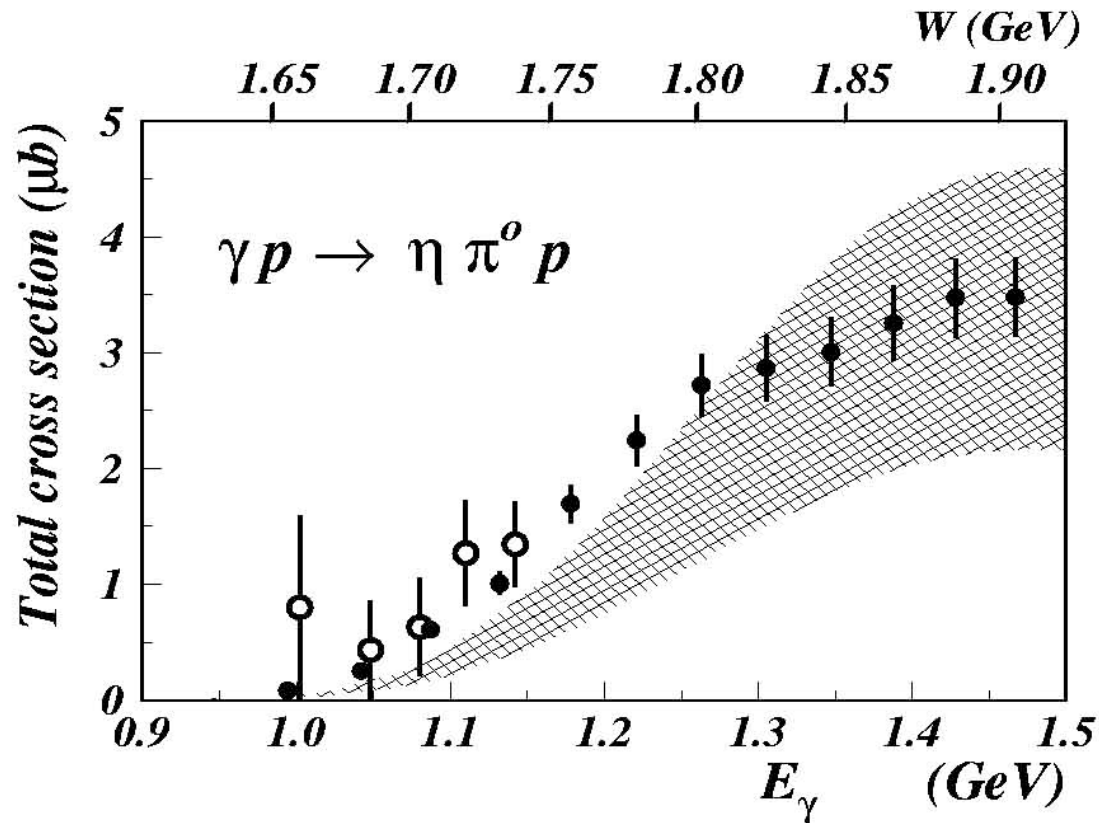

 $\sigma_{\text{tot}}$ 


FIG. 2: Total cross section of the reaction  $\gamma p \rightarrow \eta \pi^0 p$ . The dots are the experimental data of this work. The open circles are from reference [9]. The results of the model of Ref. [6, 7] are given with their uncertainty by a hatched band of the figure. The uncertainty originates from the one on the  $\gamma p \Delta(1700)$  coupling which was taken from the PDG [10]

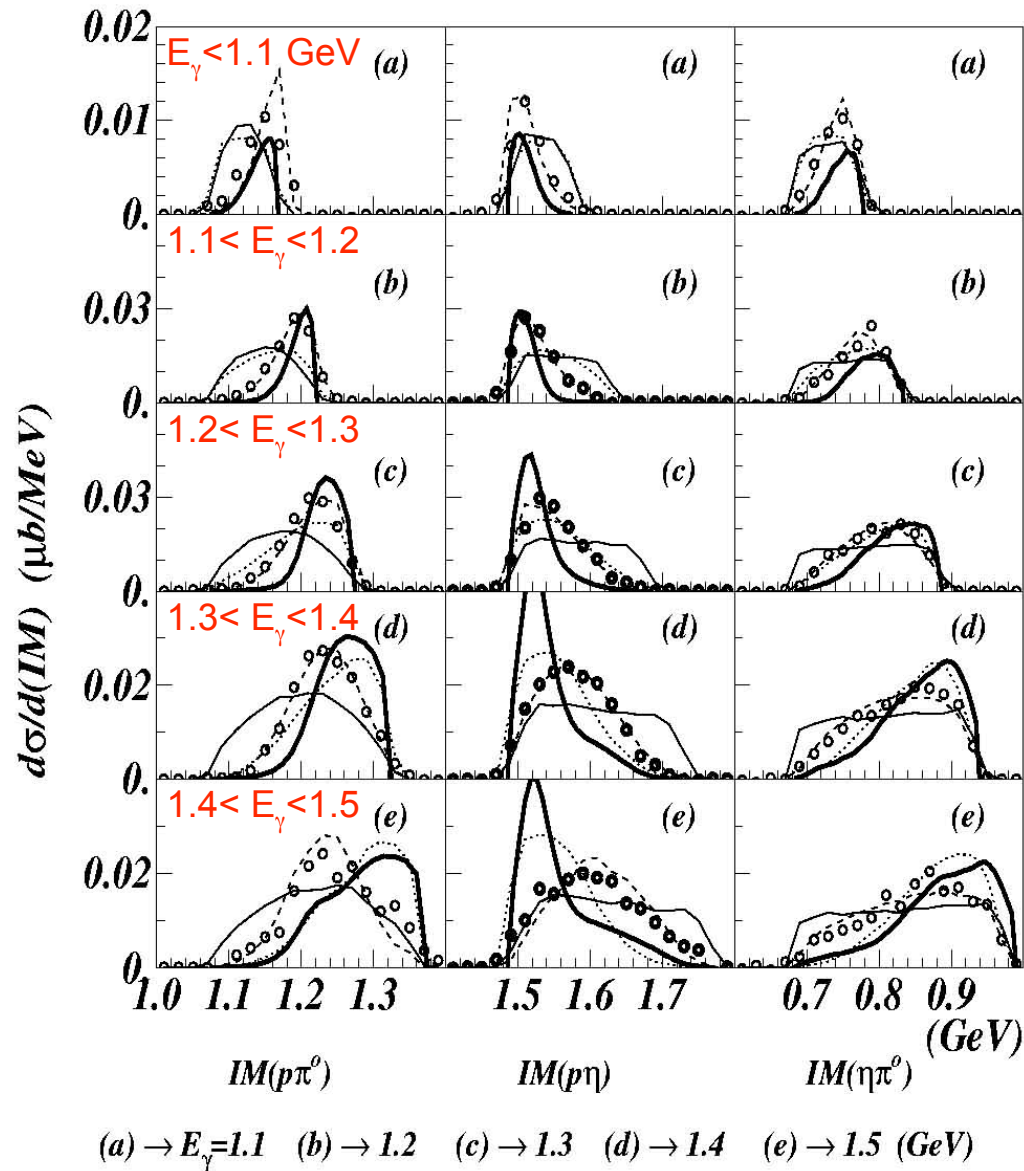
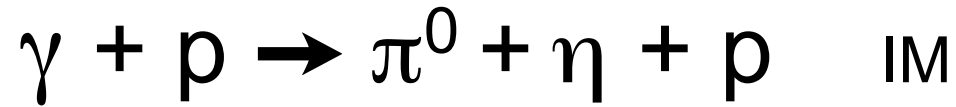
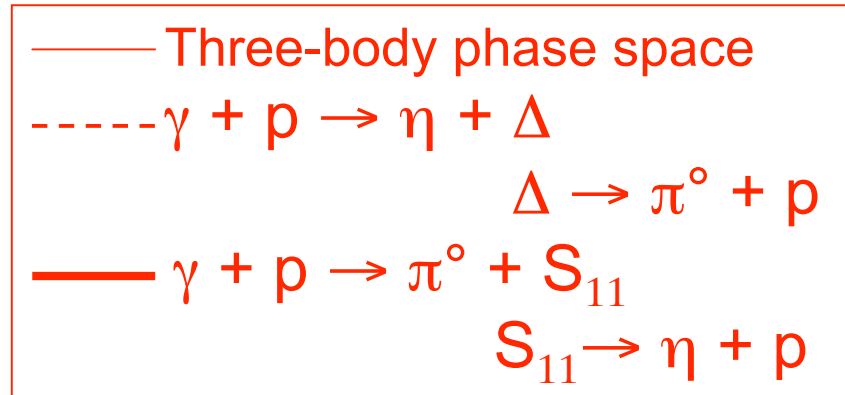
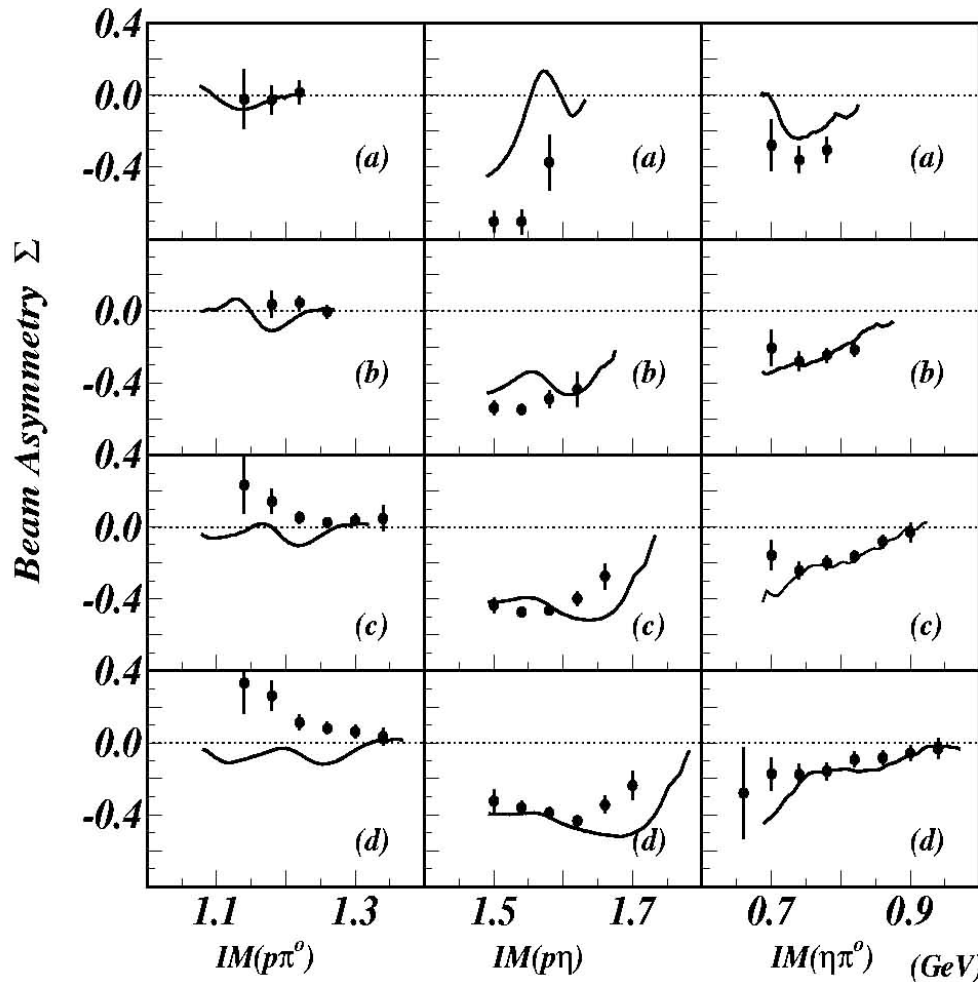
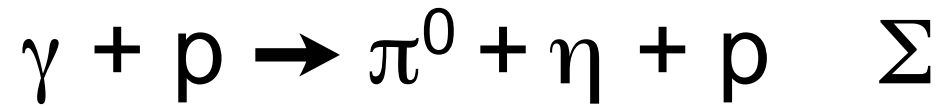


FIG. 3: For the reaction  $\gamma p \rightarrow \eta\pi^0 p$ , spectra of invariant mass of  $(p\pi^0)$ ,  $(p\eta)$  and  $(\eta\pi^0)$  groups of the final state, presented in 3 different columns. The various rows, labeled (a),..., (e) correspond to beam energies given at the bottom of the figure. In empty circles are the experimental results, in thin line for  $\gamma p \rightarrow \eta\pi^0 p$  with a 3-body phase space in the final state, in dashed line for  $\gamma p \rightarrow \eta\Delta$  with  $\Delta \rightarrow \pi^0 p$ , in dotted lines for  $\gamma p \rightarrow \pi^0 S_{11}$  with  $S_{11} \rightarrow \eta p$ . The theoretical curves, given by thick lines, are the central values of the results of the model of Ref. [6, 7].





(a)  $\rightarrow E_\gamma=1.1-1.2$  (b)  $\rightarrow E_\gamma=1.2-1.3$  (c)  $\rightarrow E_\gamma=1.3-1.4$  (d)  $\rightarrow E_\gamma=1.4-1.5$  (GeV)

FIG. 4: Beam asymmetry of the reaction  $\gamma p \rightarrow \eta \pi^0 p$ . The theoretical results are calculated with the model of Ref. [6, 7]

# K - $\Lambda$ e K - $\Sigma$

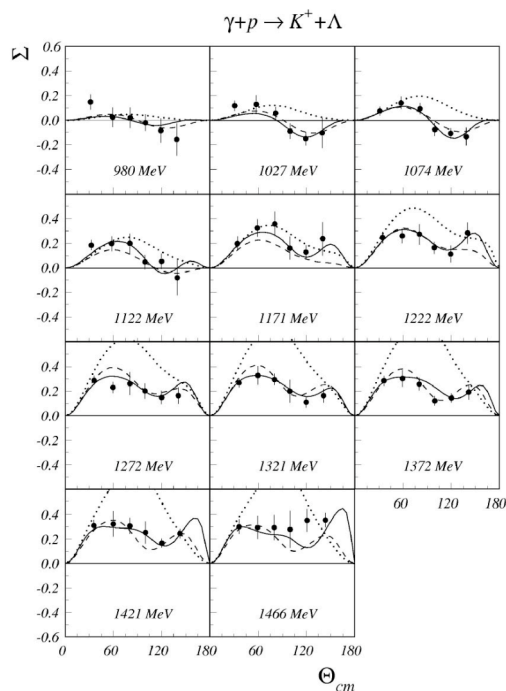


Fig. 11. Angular distributions of the beam asymmetries  $\Sigma$  for  $\gamma p \rightarrow K^+ \Lambda$  and  $\gamma$ -ray energies ranging from threshold up to 1500 MeV. Data are compared with the Bonn2005 solutions with large (dashed lines) and small (solid lines)  $S_{11}$  contribution at low energies and with the Kaon-MAID2000 standard calculation (dotted lines).

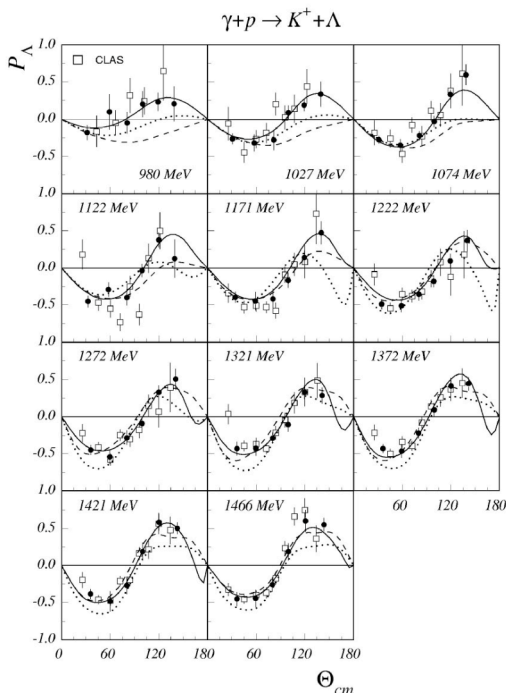


Fig. 12. Angular distributions of the  $\Lambda$  recoil polarizations for  $\gamma p \rightarrow K^+ \Lambda$  and  $\gamma$ -ray energies ranging from threshold up to 1500 MeV. GRAAL data (closed circles) are compared with CLAS data (open squares). Definition of the curves as in fig. 11.

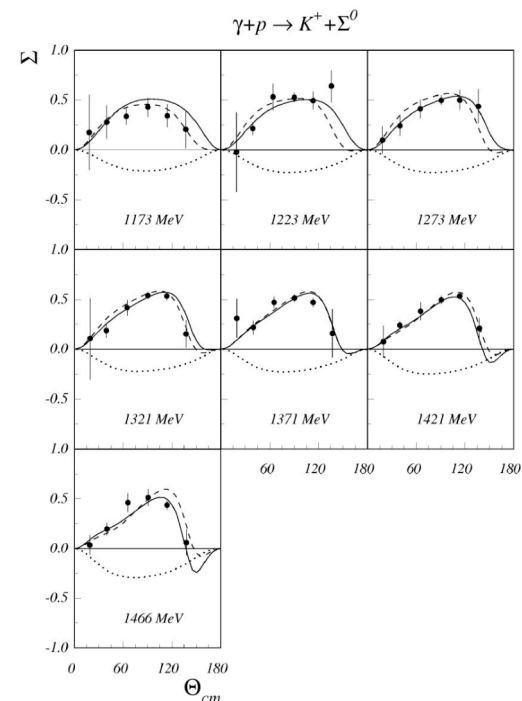


Fig. 13. Angular distributions of the beam asymmetries  $\Sigma$  for  $\gamma p \rightarrow K^+ \Sigma^0$  and  $\gamma$ -ray energies ranging from threshold up to 1500 MeV. Definition of the curves as in fig. 11.

European Physics Journal A31, 79 (2007)

Graal closed circles ●  
CLAS open squares □

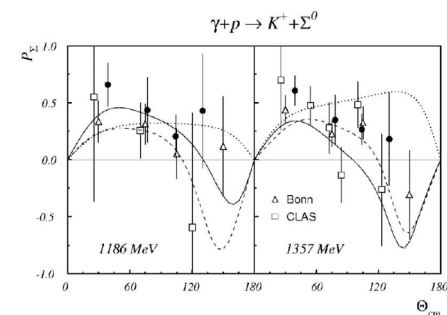
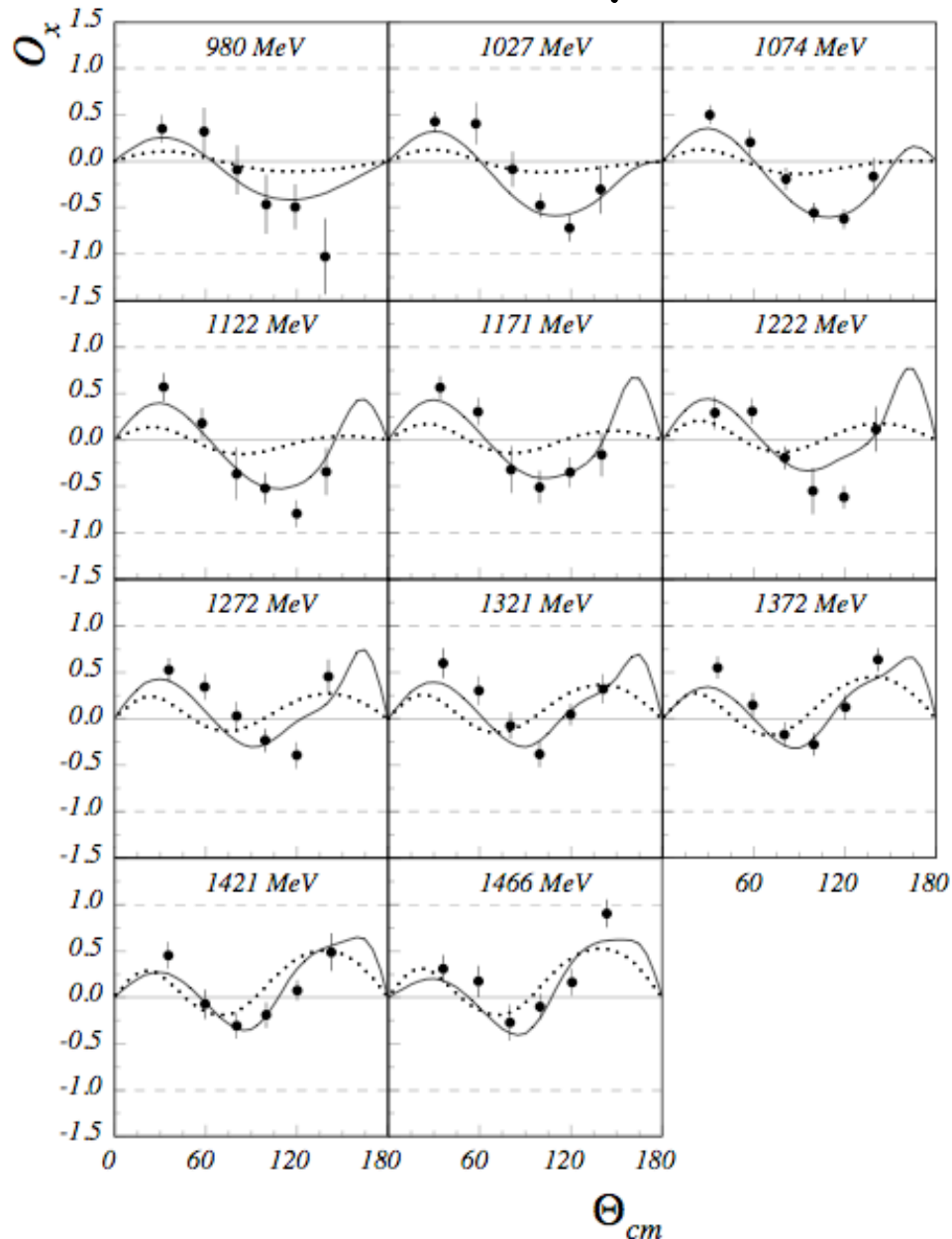


Fig. 10.  $\Sigma^0$  recoil polarizations for  $\gamma p \rightarrow K^+ \Sigma^0$ . Comparison between GRAAL (closed circles), Bonn (open triangles) and CLAS (open squares) data. Data are compared with the Bonn2005 solutions with large (dashed lines) and small (solid lines)  $S_{11}$  contribution at low energies and with the Kaon-MAID2000 standard calculation (dotted lines).



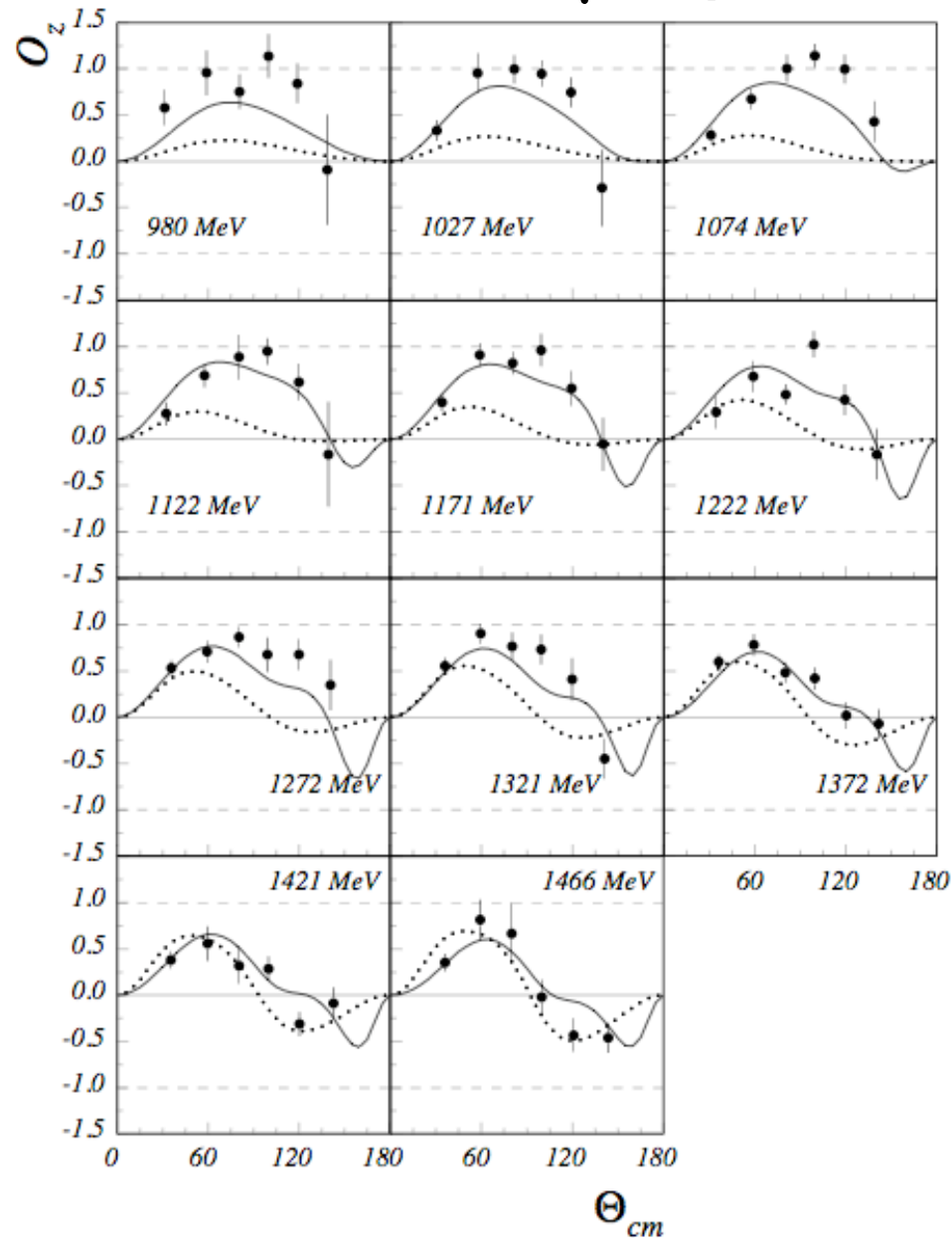
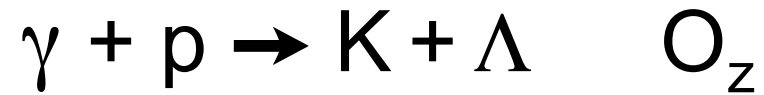


Angular distributions of the beam recoil observable  $O_x$ .

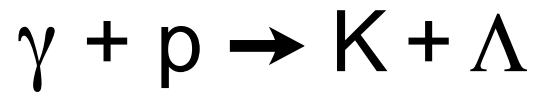
Data are compared with the predictions of two models:

**solid line BCC** (Bonn Coupled Channel - A. V. Anisovich et al. Eur. Phys. J. A 25, 427 (2005), A. V. Sarantsev et al. Eur. Phys. J. A 25, 441(2005));

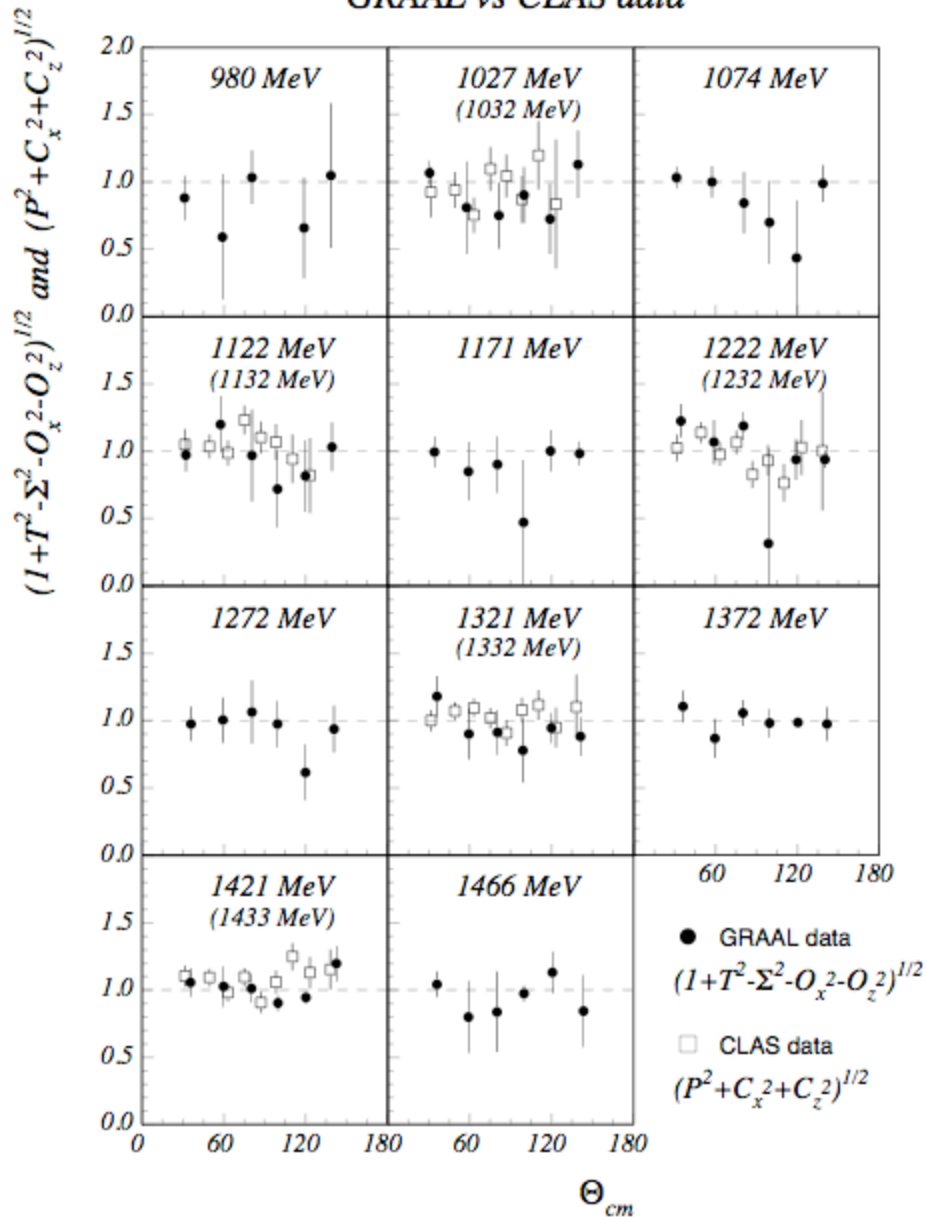
**dotted line GRPR** (Ghent Regge Plus Resonance - T. Corthals, J. Ryckerbush and T. Van Cauteren, Phys. Rev. C 73, 045207 (2006)).



Angular distributions of the beam recoil observable  $O_z$ . Data are compared with the predictions of the BCC (solid line) and GRPR (dotted line) models.



GRAAL vs CLAS data



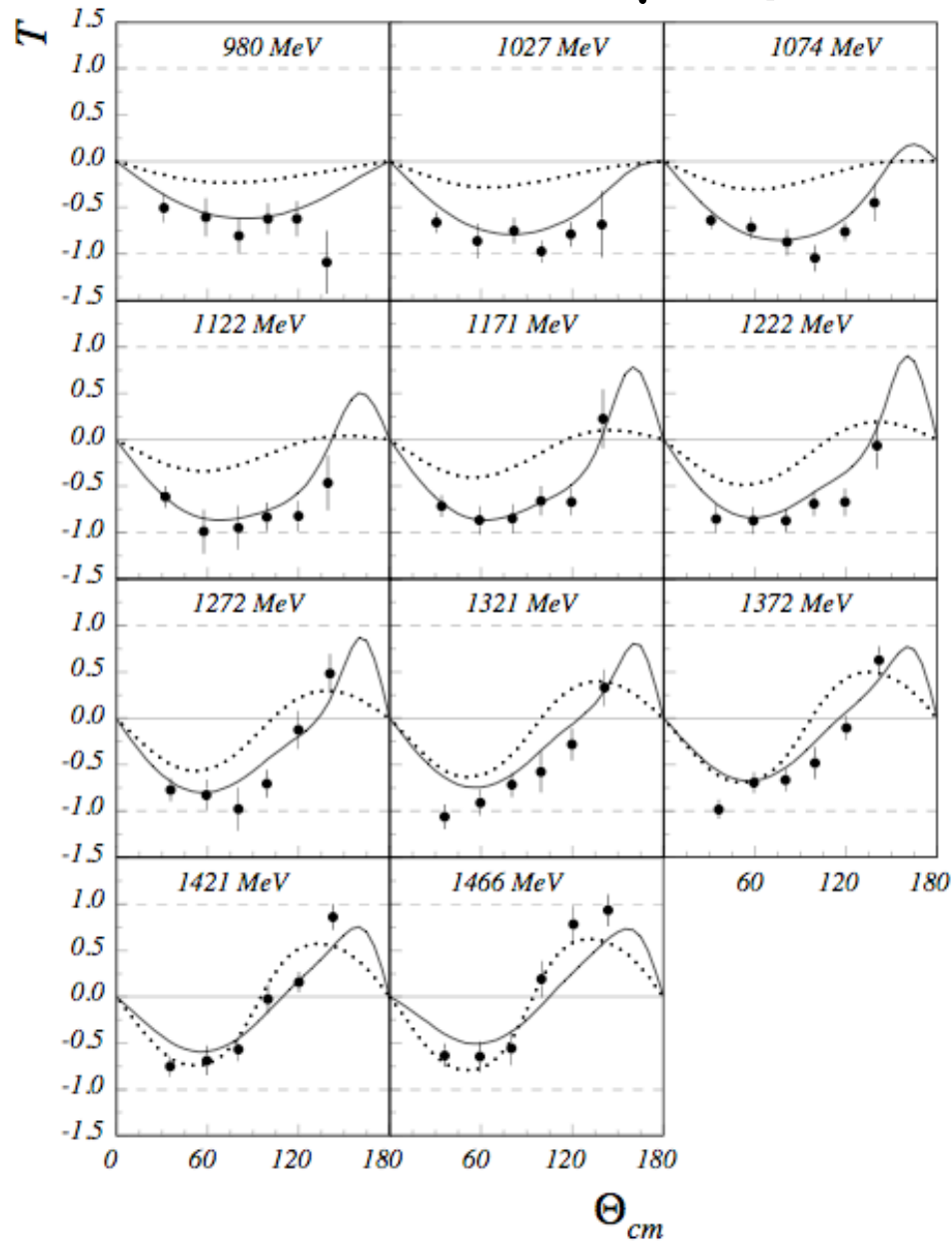
## Graal vs CLAS

Angular distributions of the quantity

$$(1 + T^2 - \Sigma^2 - O_x^2 - O_z^2)^{1/2} = (P^2 + C_x^2 + C_z^2)^{1/2}.$$

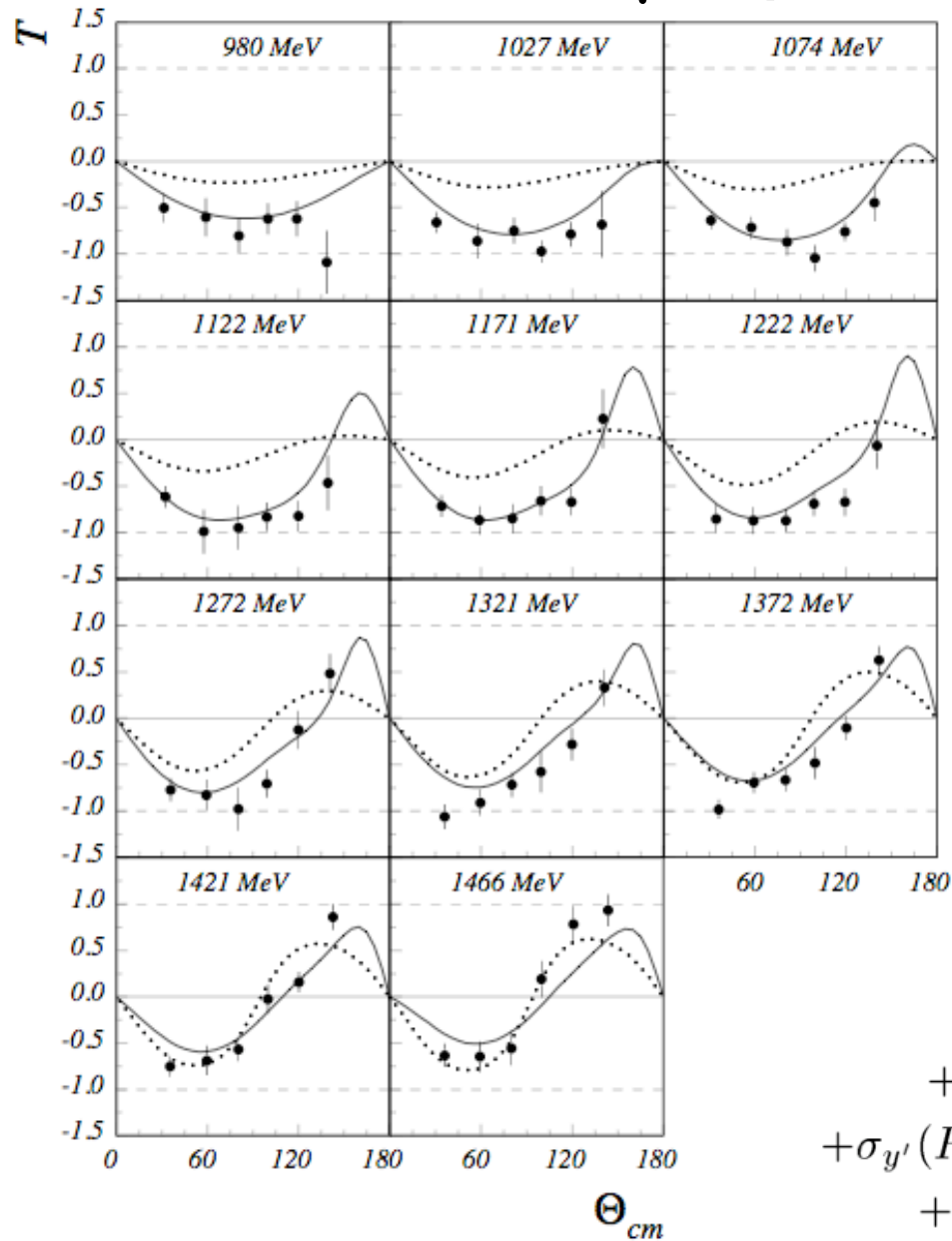
This quantity should be  $\leq 1$ .

Comparison to the values  $(P^2 + C_x^2 + C_z^2)^{1/2}$  published by the CLAS collaboration (open squares - energy in parentheses).



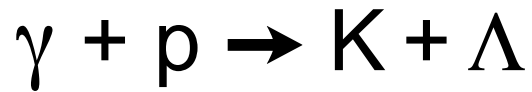
Angular distributions of the target asymmetry  $T$ .  
 Data are compared with the predictions of the BCC (solid line) and GRPR (dotted line) models.

# $\gamma + p \rightarrow K + \Lambda \quad T$

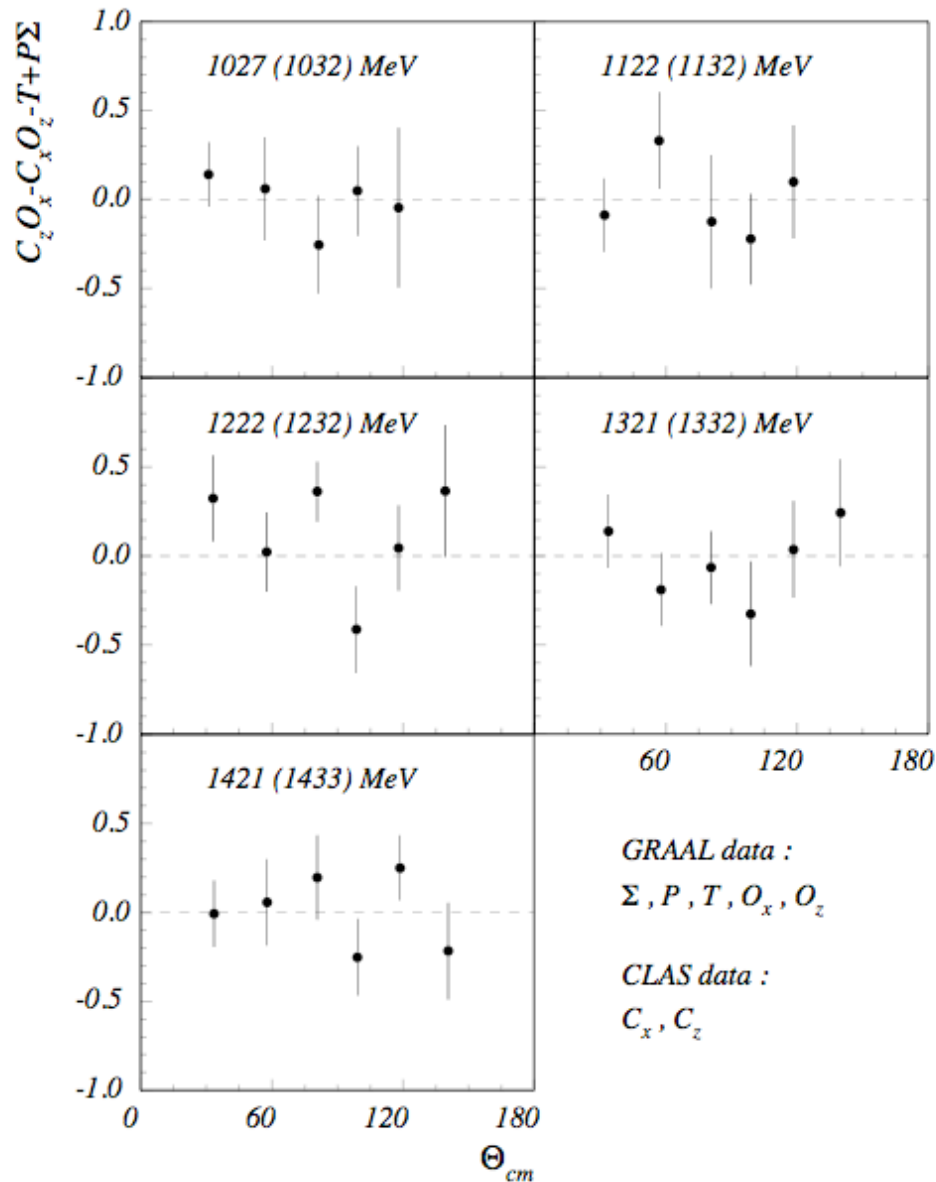


Angular distributions of the target asymmetry  $T$ .  
 Data are compared with the predictions of the BCC (solid line) and GRPR (dotted line) models.

$$\rho_f \frac{d\sigma}{d\Omega} = \frac{1}{2} \left( \frac{d\sigma}{d\Omega} \right)_0 [1 - P_\gamma \Sigma \cos 2\varphi_\gamma + \sigma_{x'} P_\gamma O_x \sin 2\varphi_\gamma + \sigma_{y'} (P - P_\gamma T \cos 2\varphi_\gamma) + \sigma_{z'} P_\gamma O_z \sin 2\varphi_\gamma]$$



GRAAL  $\times$  CLAS data



## Graal and CLAS

Angular distributions of the quantity  $C_z O_x - C_x O_z - T + P \Sigma$ .

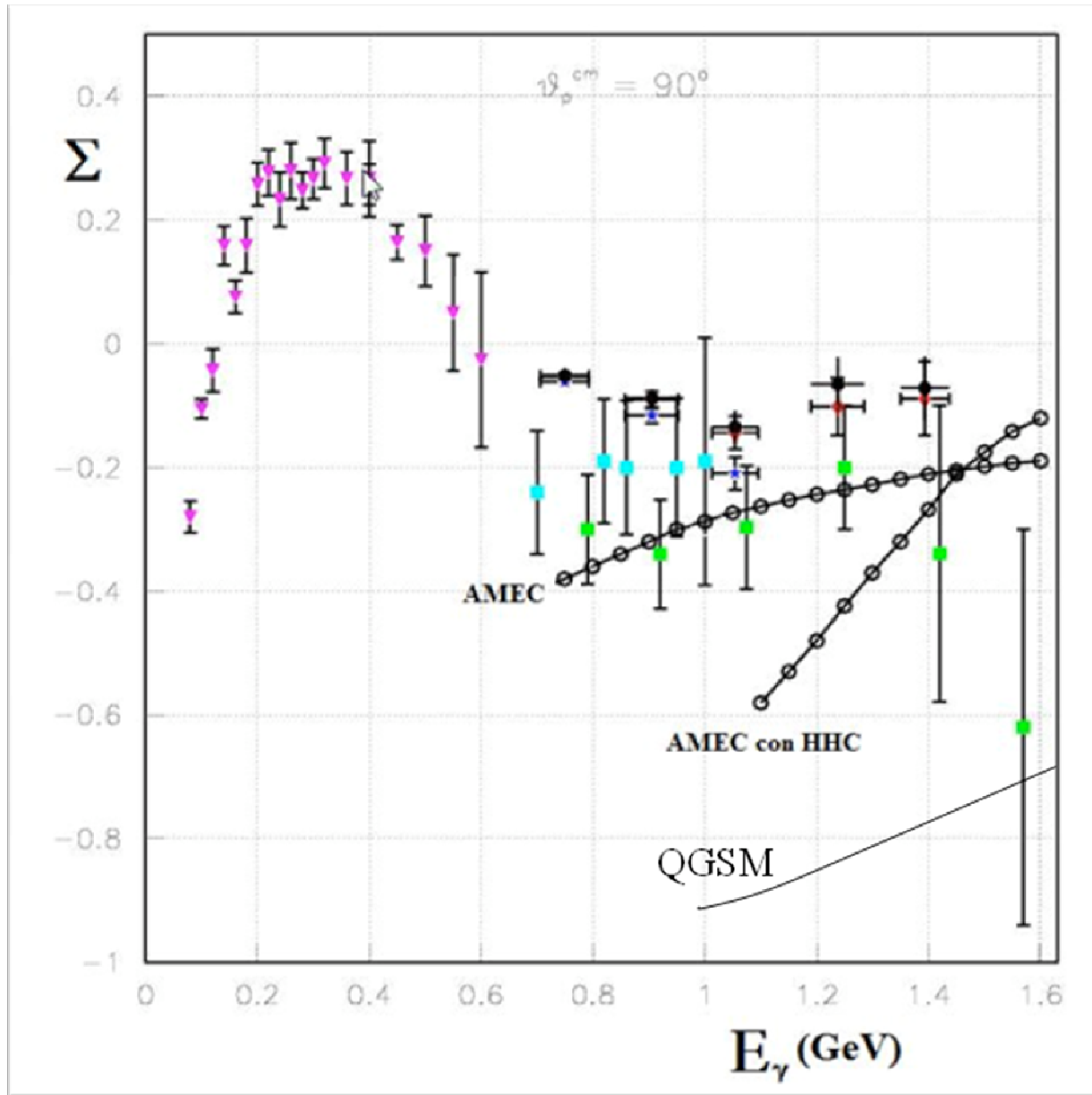
It is calculated using the  $C_x$  and  $C_z$  results published by the CLAS collaboration (energy in parentheses)

combined with our  $O_x$  and  $O_z$  data converted to have the same  $z'$  axis convention and with our  $\Sigma$ ,  $P$  and  $T$  measurements. The used CLAS data are those corresponding to the angles  $\cos(\theta_{cm})=0.85$ ,  $\text{mean}(0.65,0.45)$ ,  $\text{mean}(0.25,0.05)$ ,  $-0.15$ ,  $\text{mean}(-0.35,-0.55)$  and  $-0.75$ .

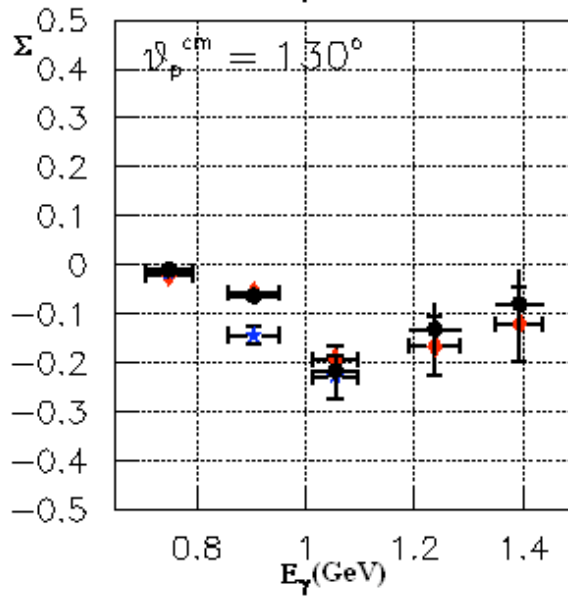
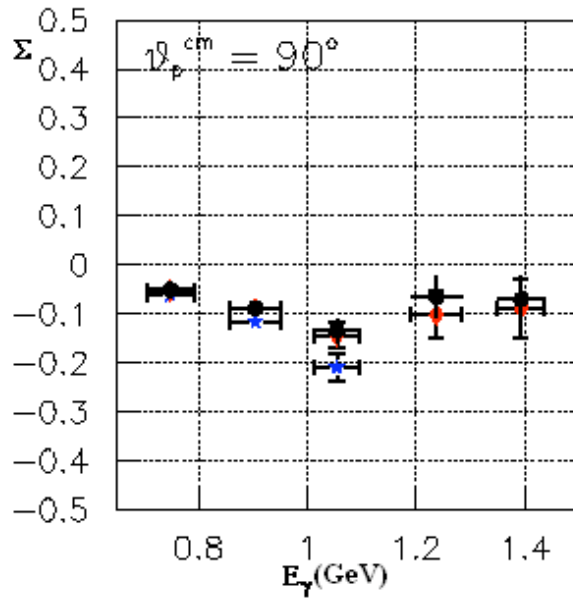
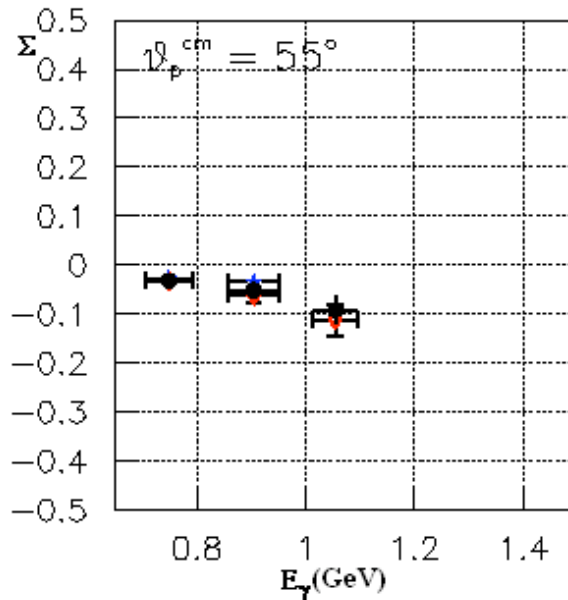
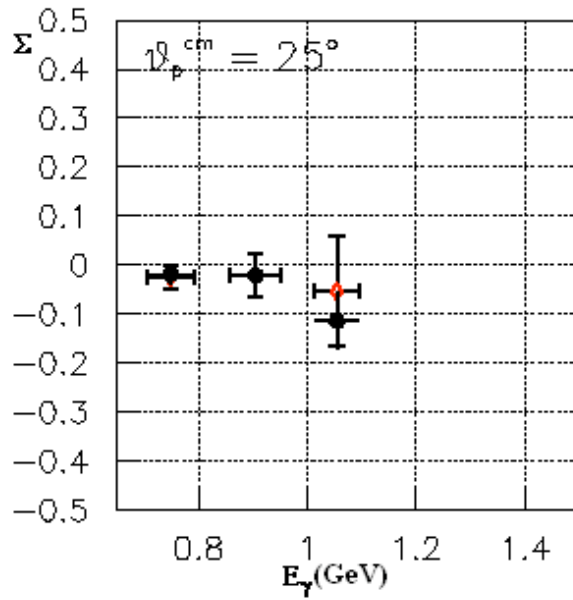
We should have the equality

$$C_z O_x - C_x O_z - T + P \Sigma = 0$$

# $\gamma + d \rightarrow p + n$    $\Sigma(90^\circ)$



- ◆ Graal data
- ▼ V. G. Gorbenko, Yu. V. Zhebrovskji et al., *Nucl.Phys.* A381 (1982) 330-342
- F. V. Adamian et al., *JETP Lett.* 39, 239 (1984)
- F. V. Adamian et al., *Eur Phys J. A* 8, 423-428 (2000)



Graal data analyzed  
in different ways

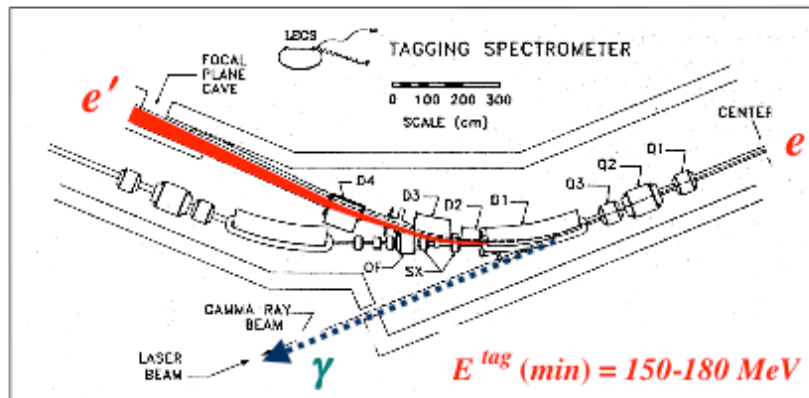
Monday, May 26, 2008

ICTP May 14, 2008



# LEGS at BNL - Summary

## Laser-Electron-Gamma-Source (LEGS)

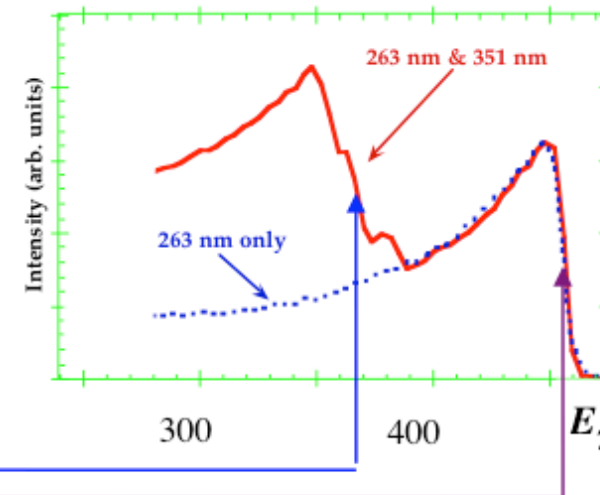


$$NSLS E_e = 2.8 GeV$$

$\gamma$  beam energy determined by  $e'$  tagging

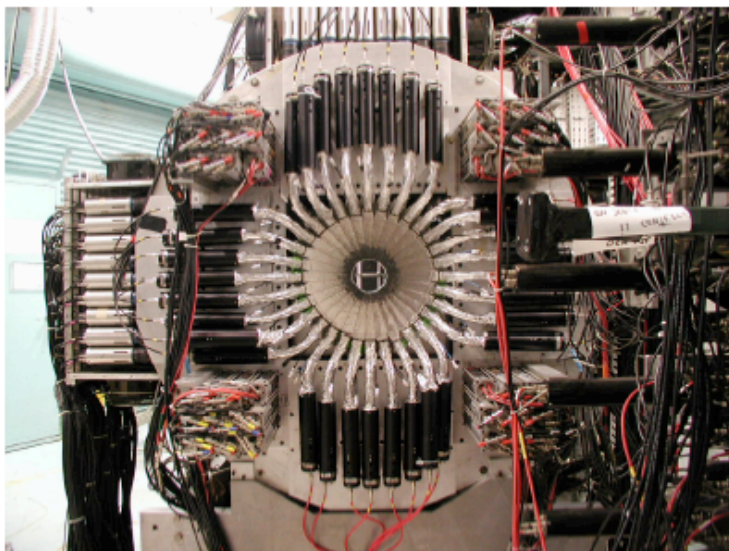
$$E_\gamma = E_e - E_{e'}, \quad \Delta E_\gamma = 3 MeV$$

	4 $\omega$ Nd-YLF ring laser	Ar-Ion laser			
$\lambda$ (nm)	263	300	351	488	515
$E_\gamma$ (max) MeV	471	421	368	275	262

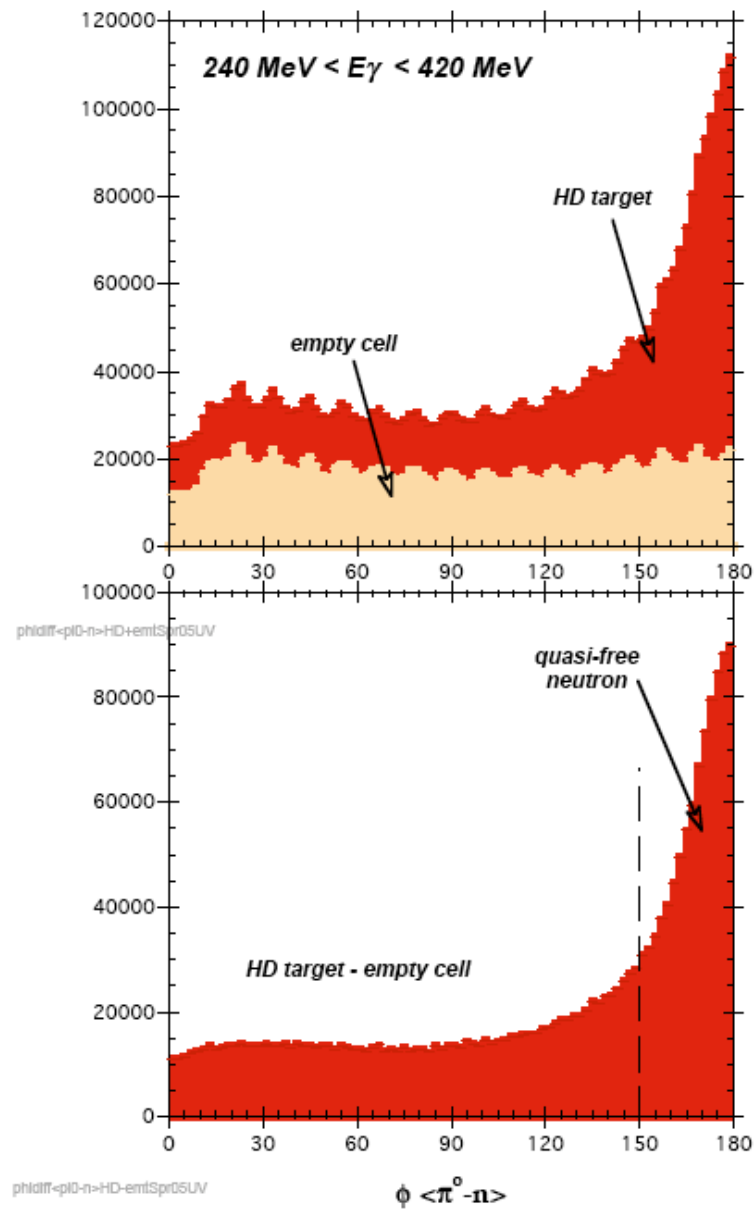


# LEGS at BNL: Spring 05 Neutron Detection

$$D(\gamma, \pi^0 n) p$$



neutron-barrel  
(U Roma-II)



# LEGS at BNL: Target Polarization

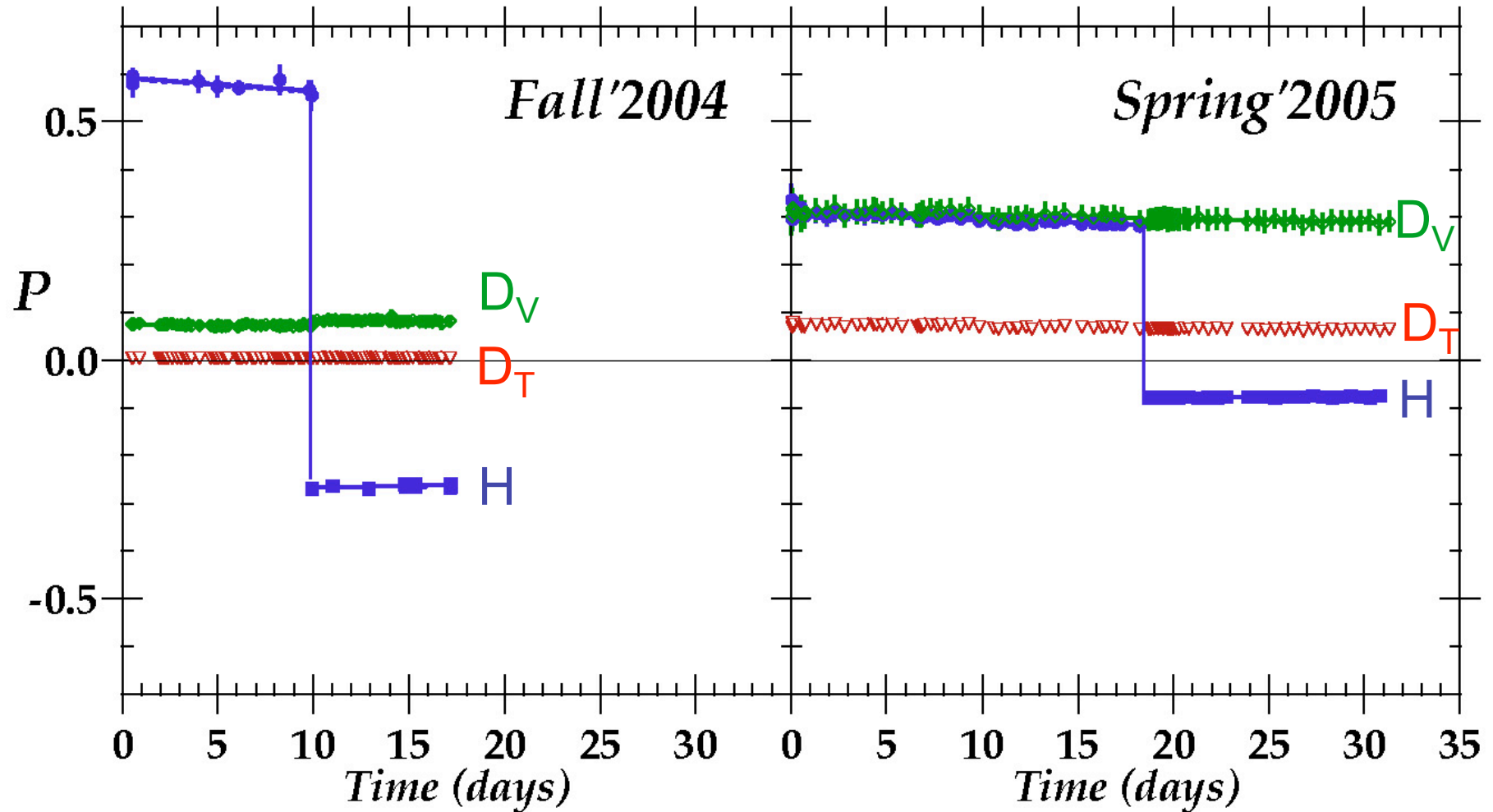
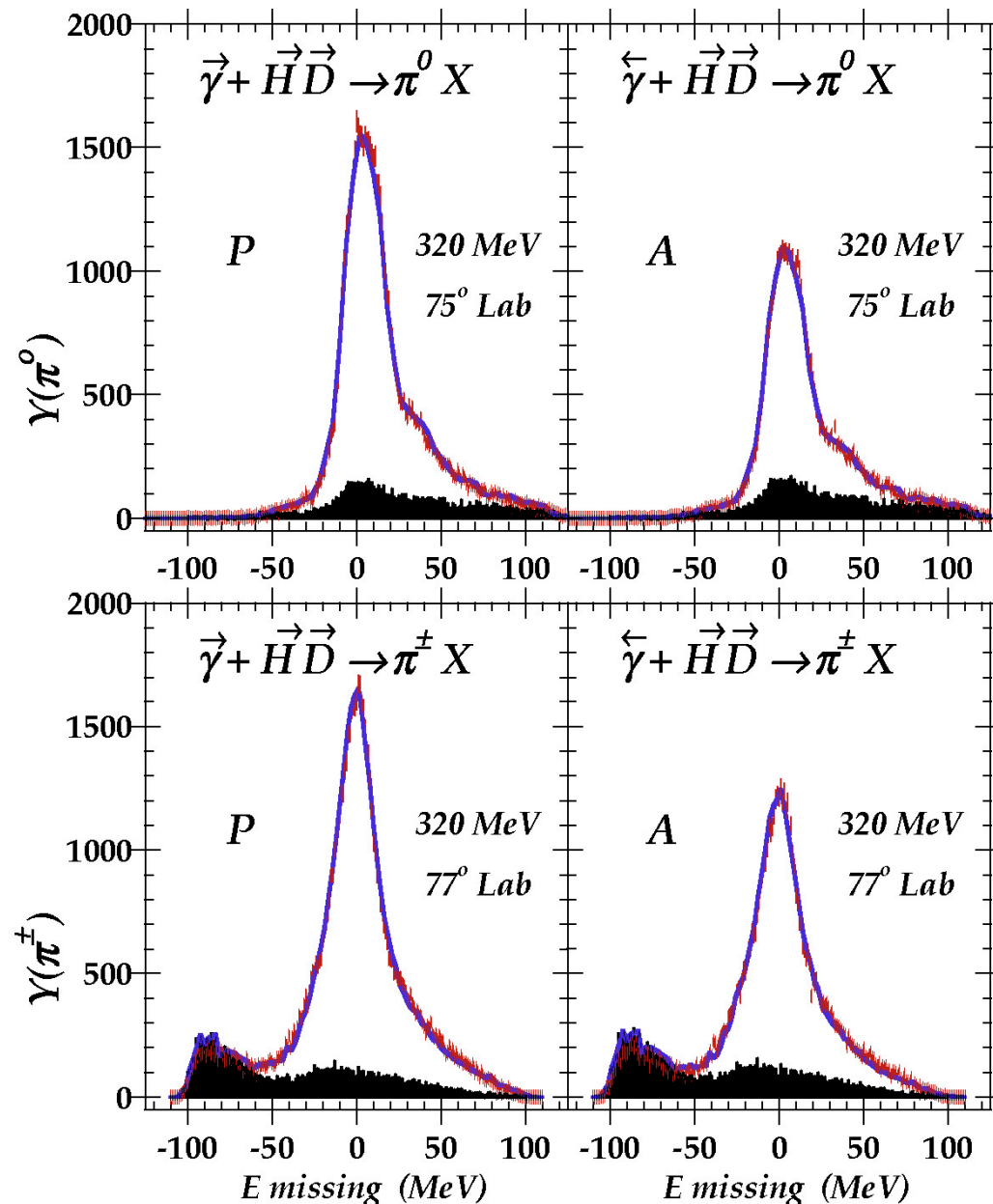


Figure 1. Polarizations of H (blue) and D (green-vector and red-tensor) nuclei in HD during the two data collection periods. Mid-way through each, the H polarization was flipped using an RF transition.

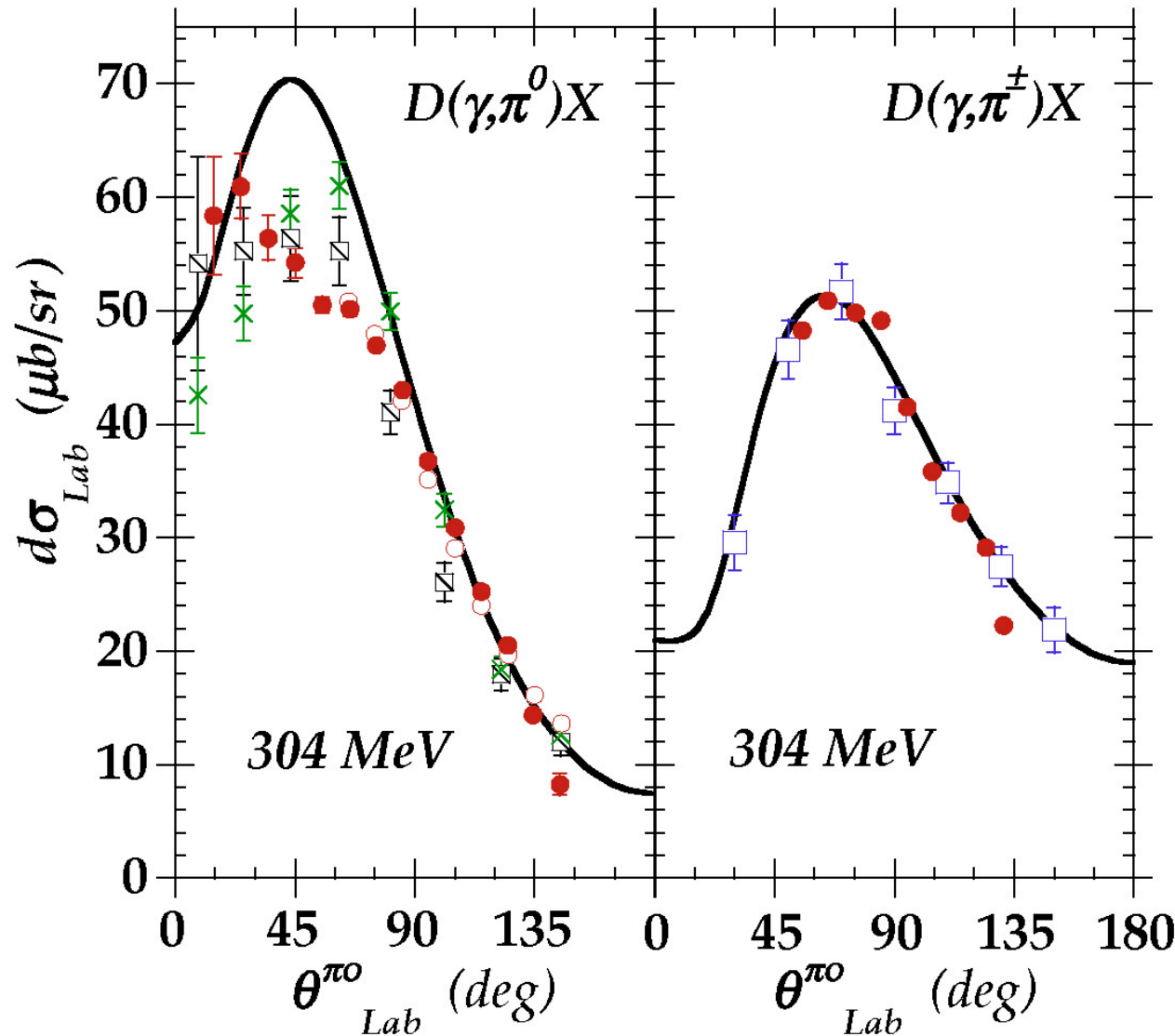
# LEGS at BNL: $H/D(\gamma, \pi^{0/\pm})$



Differences between 2-body kinematics and the measured energy for  $\pi_0$  (top panels) and  $\pi_\pm$  (bottom panels), in the cases of parallel (left panels) and anti-parallel (right panels) beam and target spin alignments. The simulated energy differences are shown as the solid curves.

PRELIMINARY

# LEGS at BNL: $D(\gamma, \pi^{0/+})$



Unpolarized cross sections (solid circles) for  $D(\gamma, \pi^0)X$ , left panel, and  $D(\gamma, \pi^\pm)X$ , right panel, at  $E_\gamma = 304$  MeV, deduced by subtracting SAID predictions[8] for  $p(\gamma, \pi)$  from the fitted results for HD. For the  $\pi^0$  channel, LEGS data from a liquid  $D_2$  target are shown as open circles, while crosses and hatched-boxes are TAPS data from [18] and [17]. For the  $\pi^\pm$  channel, open boxes are constructed from  $\pi$ -pp [19] and the  $\pi^-/\pi^+$  ratio data of [20]. The curves are calculations from Fix and Arenhövel [12].

**PRELIMINARY**

# LEGS at BNL: $H(\gamma, \pi^{0/+})$

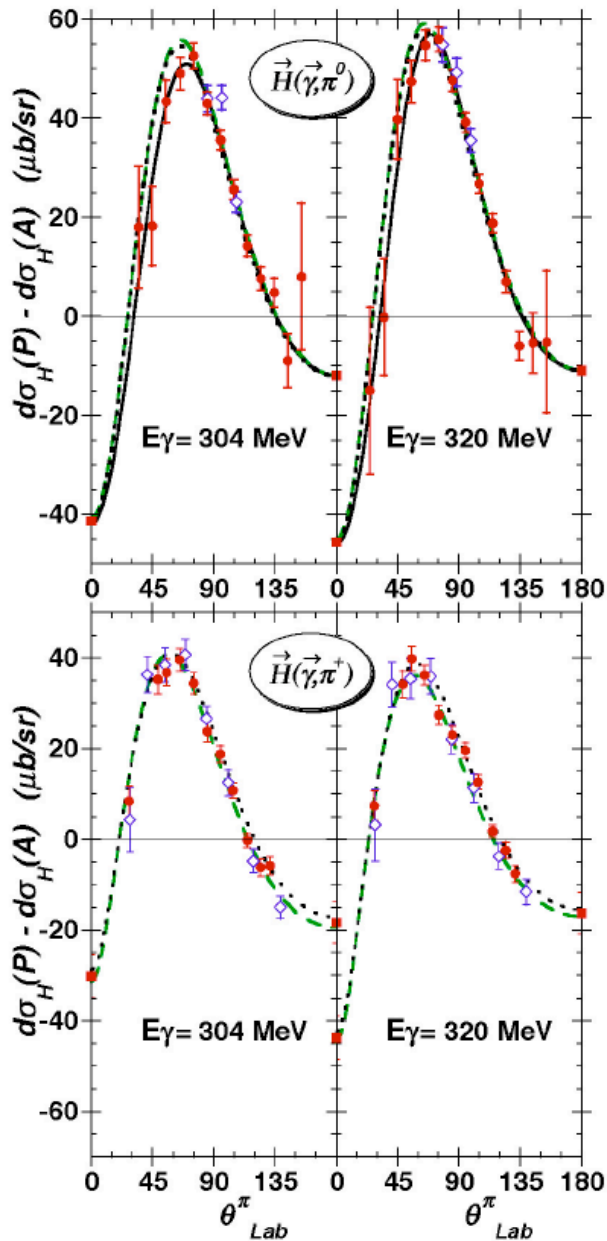


Figure 4. Angular dependence of the  $[d\sigma(P) - d\sigma(A)]$  spin-difference cross section for polarized H at beam energies near the  $\Delta$  peak. The full data from Fall'04 and Spring'05 are shown as solid circles. Unpolarized limits (solid squares) at  $0^\circ$  and  $180^\circ$  are the mean of SAID[8] and MAID[9]. Open diamonds are results from Mainz [21] at 310 MeV (left) and at 330 MeV (right). Predictions from SAID and MAID are shown as dotted and dashed curves, respectively. The solid curves in the top panels are a Legendre fit to the new data.

PRELIMINARY

# Compton Scattering Kinematics

2. The maximum energy lost by the electrons after an elastic scattering with a laser photon is given by the maximum energy acquired by the photon:

$$E_{el}^0 - E_{el}^{scatt} = E_{\gamma \max} = \frac{4\gamma^2 E_{laser}}{1 + \frac{4\gamma E_{laser}}{m_e}} \approx 4\gamma^2 E_{laser}$$

This energy loss is measured by the displacement  $d$  of the scattered electrons from the primary electron beam after the first magnetic dipole. For the ESRF electron energy of 6.03 GeV and a UV laser line of 3.53 eV, the energy loss is 1.487 GeV and corresponds to an electron displacement at the position of the Graal tagging detector:  $d \approx 52.3$  mm.

The microstrips of the Graal tagging detector measure the displacement  $d$  of the scattered electrons from the main orbit and therefore the energy lost by the electrons (and acquired by the gamma-rays):

$$E_{\gamma} \propto d$$

## Compton Scattering Kinematics

3. From the relativistic kinematics of Compton scattering:

$$E_{\gamma \max} = \frac{4\gamma^2 E_{laser}}{1 + \frac{4\gamma E_{laser}}{m_e}} \approx 4\gamma^2 E_{laser} \quad \text{and} \quad \frac{dE_\gamma}{E_\gamma} \approx 2 \frac{d\gamma}{\gamma} \quad \text{or} \quad \frac{d\gamma}{\gamma} \approx \frac{1}{2} \frac{dE_\gamma}{E_\gamma}$$

and in general from relativistic kinematics:

$$\beta d\beta = \left( \frac{1}{\gamma^2} \right) \frac{d\gamma}{\gamma} \approx \frac{1}{2} \left( \frac{1}{\gamma^2} \right) \frac{dE_\gamma}{E_\gamma} \quad \text{or} \quad \Delta\beta \approx \frac{1}{2} \left( \frac{1}{\gamma^2} \right) \frac{\Delta E_\gamma}{E_\gamma}$$

since at the ESRF:

$$\gamma = \frac{E_e}{m_e} = \frac{6030}{0.511} = 11\,800; \quad 2\gamma^2 \approx 2.8 \cdot 10^8$$

we have:

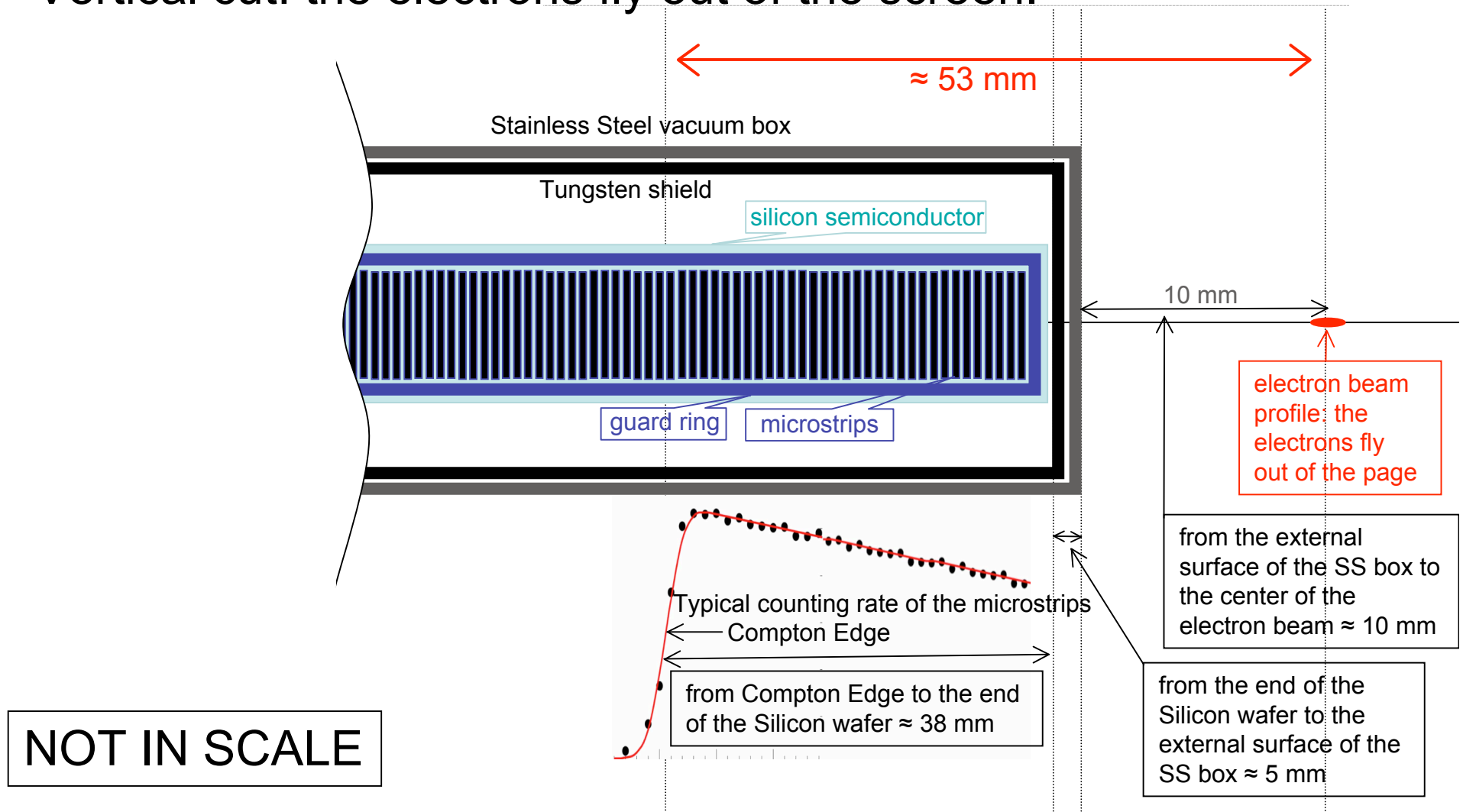
$$\Delta\beta \approx \frac{1}{2} \left( \frac{1}{\gamma^2} \right) \frac{\Delta E_\gamma}{E_\gamma} \approx \frac{1}{2.8 \cdot 10^8} \cdot \frac{\Delta E_\gamma}{E_\gamma} \approx 0.4 \cdot 10^{-8} \frac{\Delta E_\gamma}{E_\gamma} \approx 0.4 \cdot 10^{-8} \frac{\Delta d}{d}$$

The error in  $\beta$  is reduced by eight orders of magnitude with respect to the relative error in  $d$  (the displacement of the scattered electrons from the main orbit).

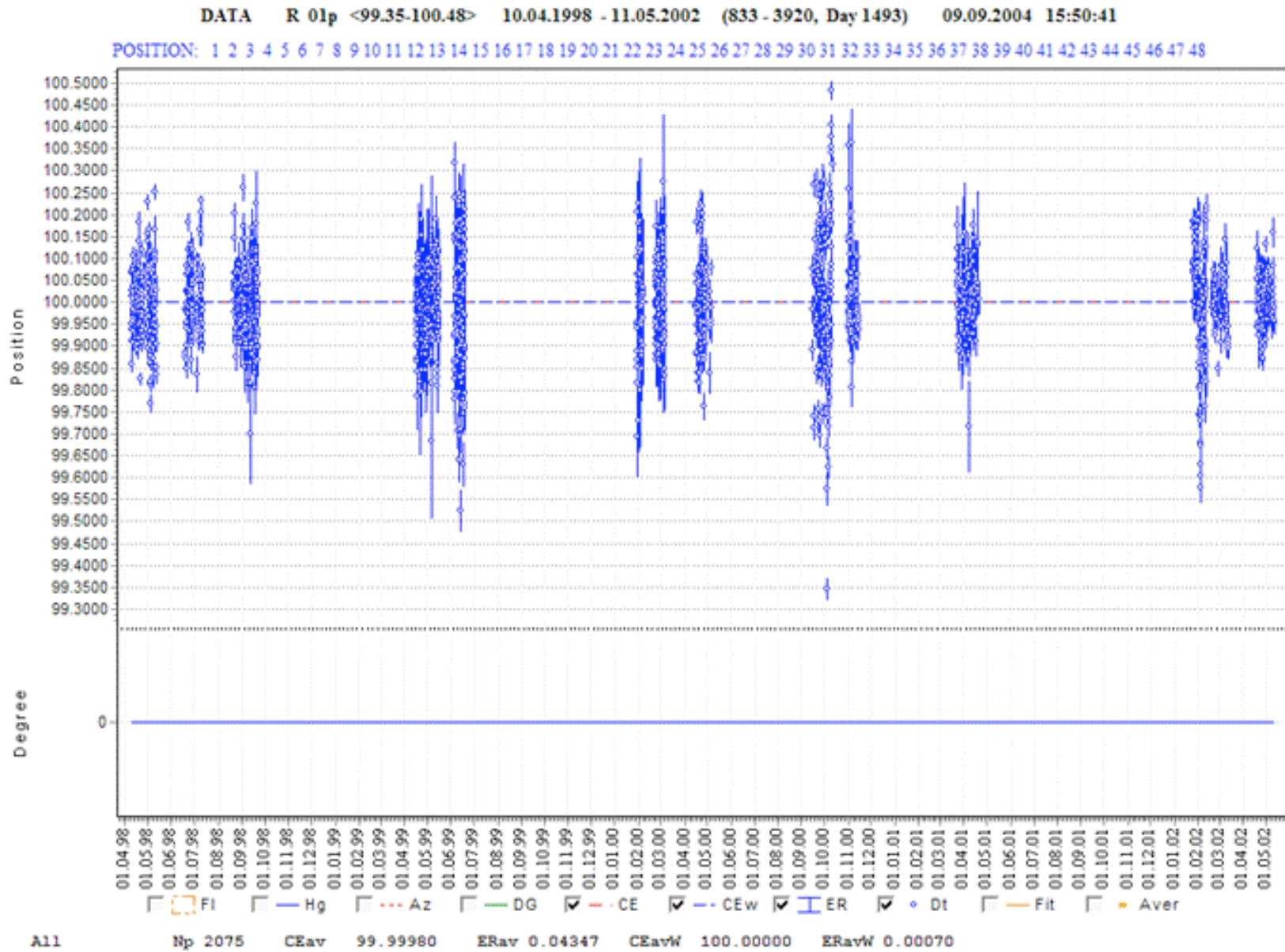


# Graal Tagging Microstrips

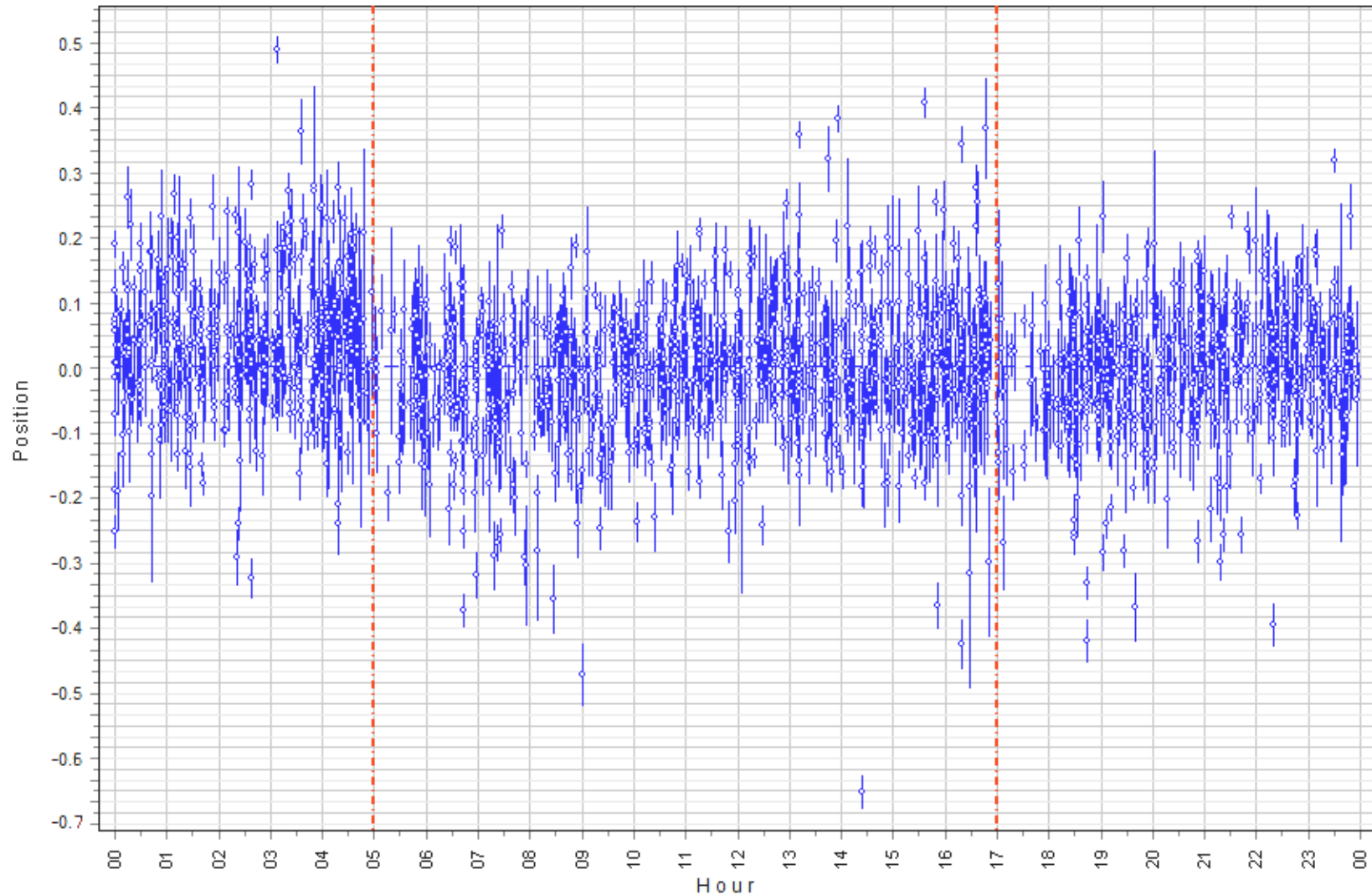
Schematic description of the tagging detector in more details.  
Vertical cut: the electrons fly out of the screen.



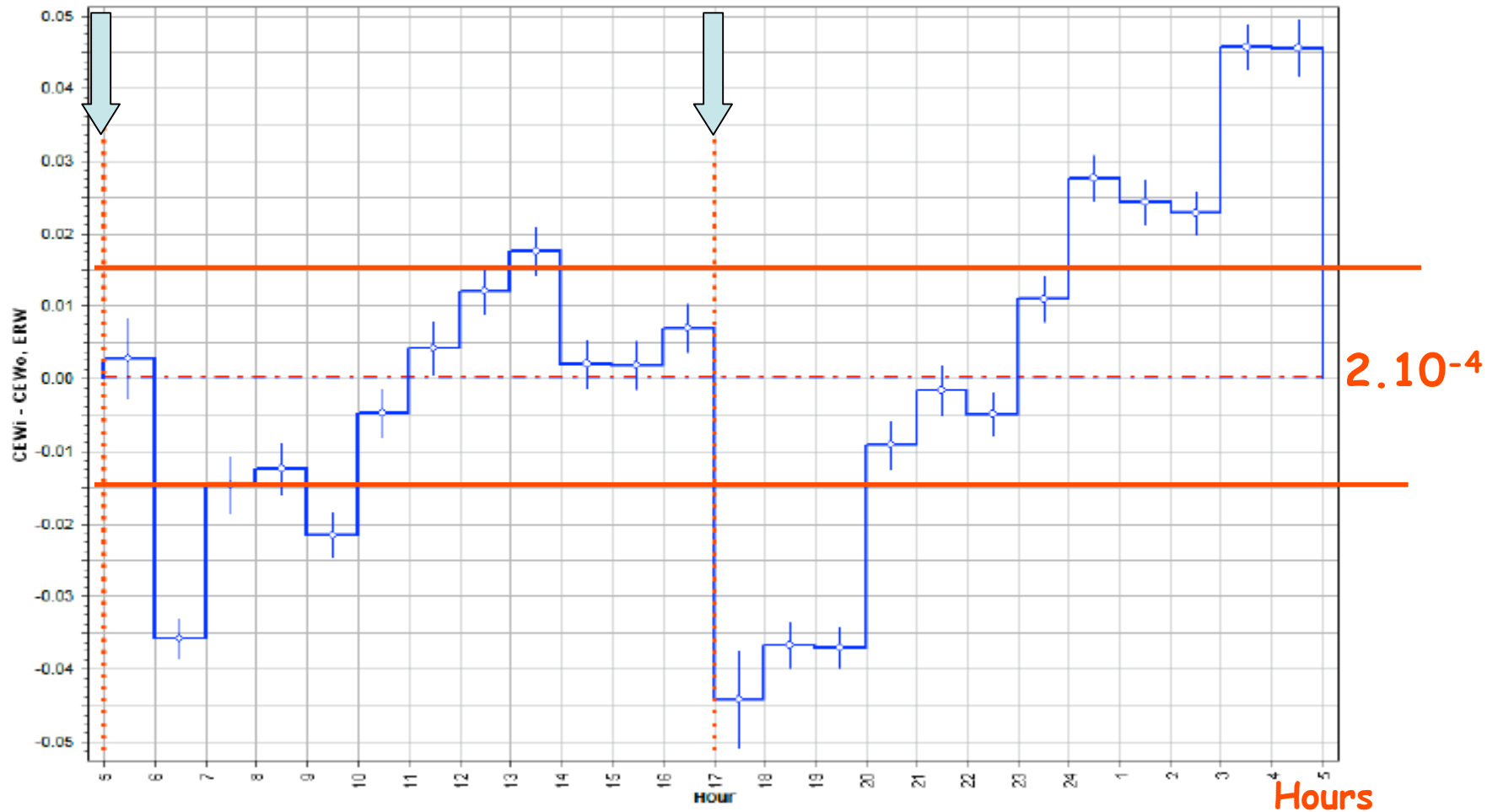
# Distribution of Graal Data



# Daily Compton Edges Distributions



Experimental data plotted as a function of (solar) hour, showing their daily variation. The dispersion of data around the average, taken arbitrarily at zero, is expressed in fractions of microstrip (300 micrometers width or about 7 MeV for one microstrip).



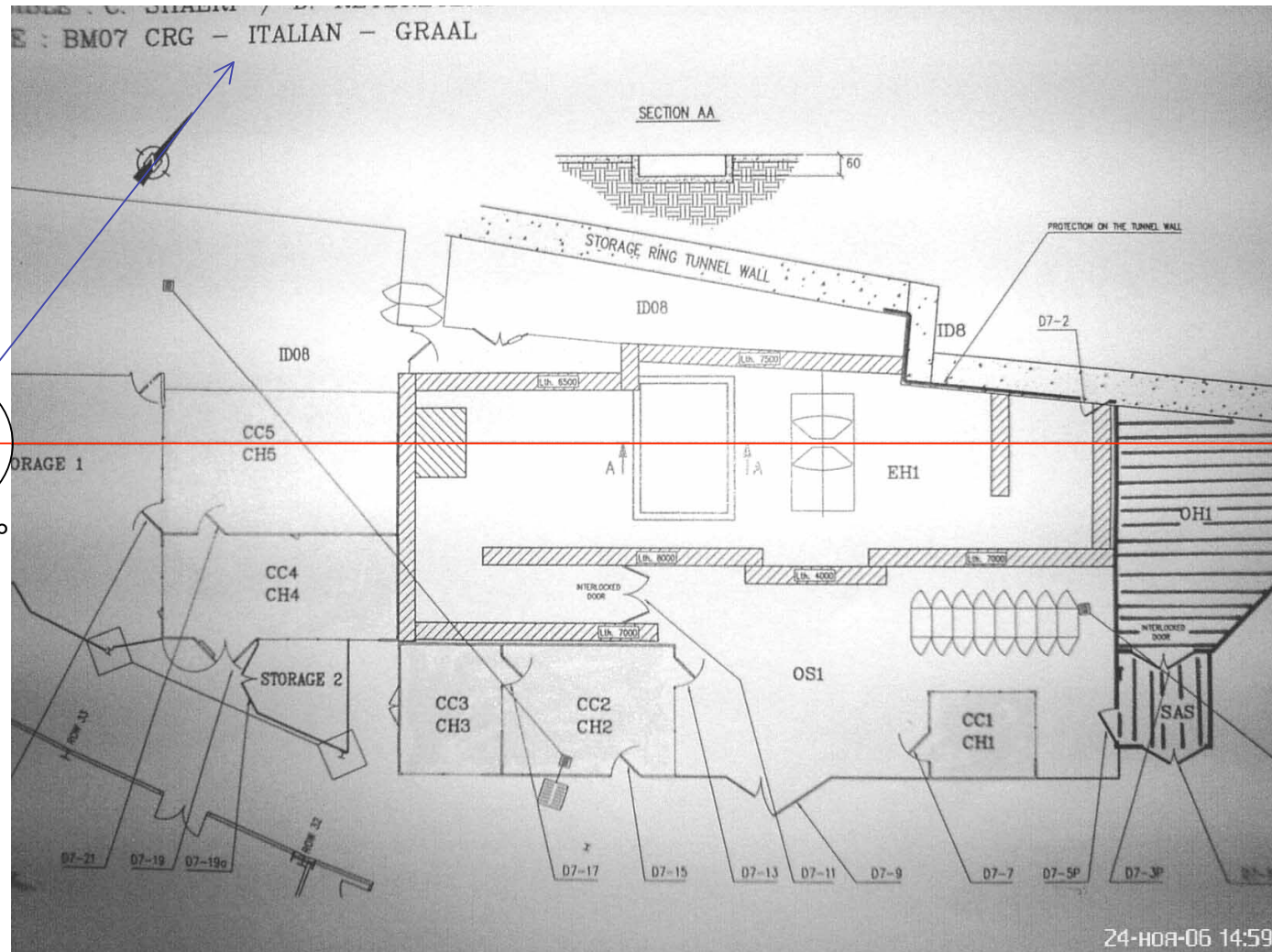
Same as the previous figure, but each point is the average over one hour. The dotted lines show the refill time of the machine corresponding to a possible change in the temperature of the tagging detector or the position of the beam. The average is expressed in microstrip fractions ( $0.01 = 3\mu\text{m}$ ).

# Graal Beam Orientation on the Earth

The Graal beam points approximately to the S-W

≈S-W  
(225°)

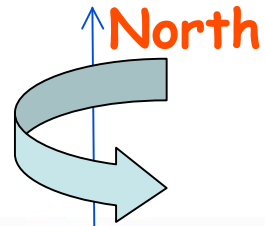
230.6°



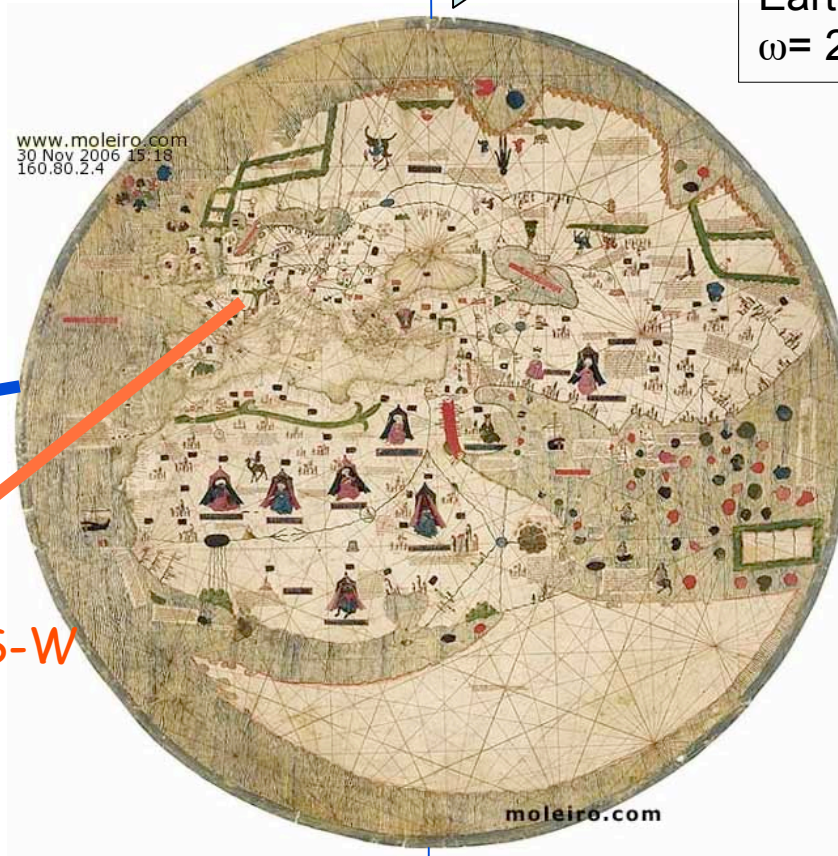
Earth rotation around its axis:  $\omega = 7.3 \cdot 10^{-5} \text{ rad s}^{-1}$

Earth rotation around the sun:  $\omega = 2 \cdot 10^{-7} \text{ rad s}^{-1}$

# Graal Rotations and the CMB



Earth rotation around its axis:  
 $\omega = 7.3 \cdot 10^{-5} \text{ rad s}^{-1}$   
Earth rotation around the sun:  
 $\omega = 2 \cdot 10^{-7} \text{ rad s}^{-1}$

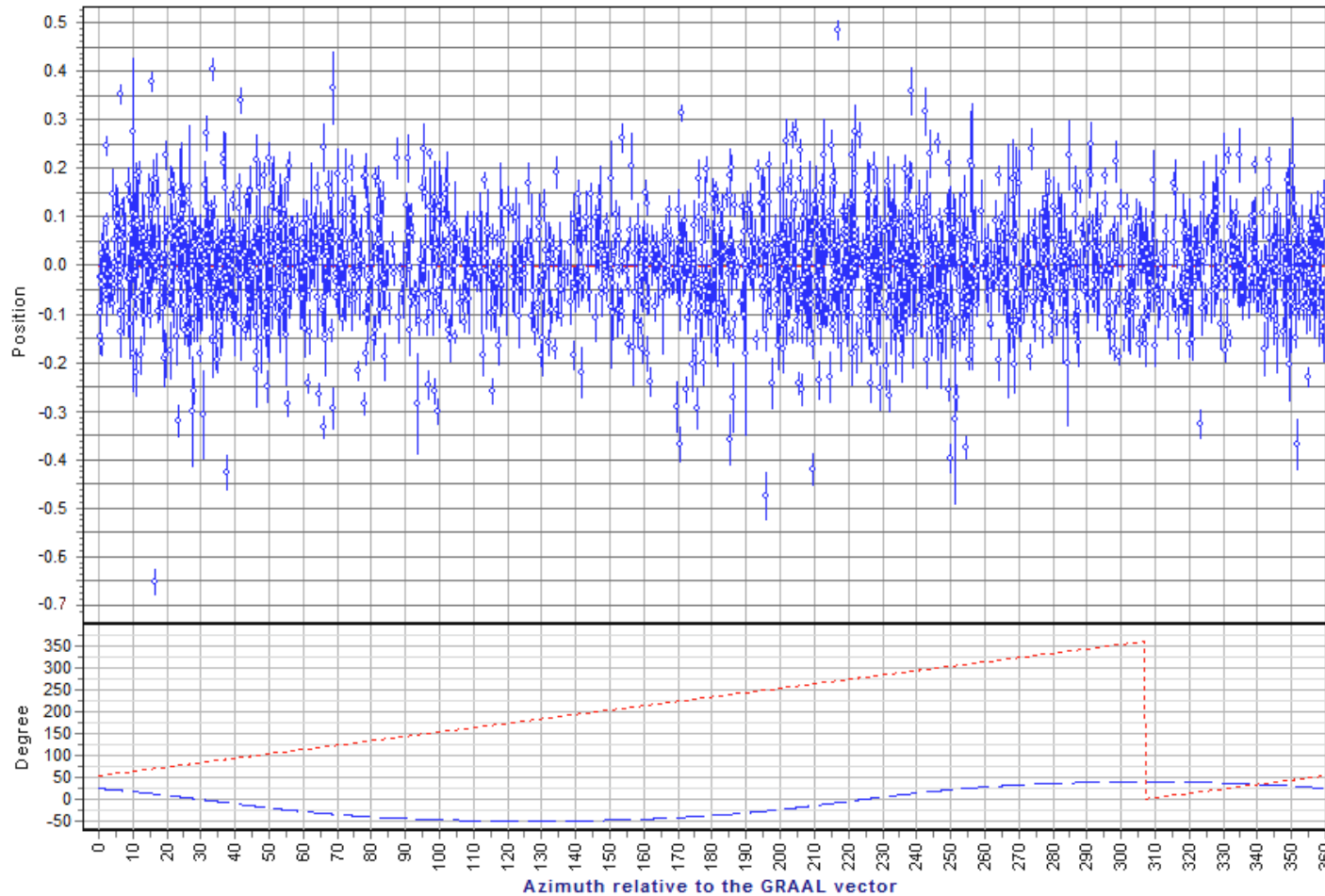


CMB (97° / NS Axis)

GRAAL beam line  
approximately to the S-W

mappamondo estense 1450

# Compton Edge Positions vs CMB Dipole



Experimental data plotted as a function of the azimuth (above); below, the variation of the angle between the beam and the CMB dipole decomposed to azimuth (dotted) and declination (dashed) angles is shown.

## Preliminary Result

Assuming an error of

$$2 \cdot 10^{-4}$$

in our determination of the position of the Compton Edge, we could arrive to an estimated upper limit on the asymmetry of the velocity of light of:

$$\Delta\beta \approx \frac{1}{2} \left( \frac{1}{\gamma^2} \right) \frac{\Delta E_\gamma}{E_\gamma} \approx 0.4 \cdot 10^{-8} \frac{\Delta d}{d} \approx 0.4 \cdot 10^{-8} \cdot 2 \cdot 10^{-4} \approx 10^{-12}$$

Considering that we have analyzed old data and we have not been able to reconstruct completely the status of the system - accelerator + tagging detector - during our runs we have published the more conservative number:

$$3 \cdot 10^{-12}$$



## An Optimistic View of the Future

In conclusion if optimistically we assume a systematic error of  $2.5 \mu\text{m}$  in the distance between the position of the Compton Edge and the electron beam, we have:

$$\frac{(\Delta d)_{\text{sys}}}{d} \approx \frac{2.5 \mu\text{m}}{52.3 \text{mm}} \approx 5 \cdot 10^{-5} \approx \frac{(\Delta E_{\gamma})_{\text{stat}}}{E_{\gamma}}$$

and we can hope to be able to verify the isotropy of the velocity of light with respect to some absolute reference frame with a precision of:

$$\Delta\beta \approx \frac{1}{2} \left( \frac{1}{\gamma^2} \right) \frac{\Delta E_{\gamma}}{E_{\gamma}} \approx 0.4 \cdot 10^{-8} \frac{\Delta E_{\gamma}}{E_{\gamma}} \approx 0.4 \cdot 10^{-8} \cdot 5 \cdot 10^{-5} \approx 2 \cdot 10^{-13}$$